Chinese Journal of Natural Medicines

Artemisinin derived from *Artemisia annua* L. promotes thrombopoiesis *via* targeting FLT3: a novel strategy for thrombocytopenia management

Xinyue Mei, Sheng Liu, Linglin Zhou, Yiling Wang, Tianci Hu, Xiao Qi, Fengyu Li, Feihong Huang, Wenchuan Peng, Xinyue Shen, Siyu Huang, Mengying Lei, Anguo Wu, Jianming Wu, Jiesi Luo, Long Wang

Citation: Xinyue Mei, Sheng Liu, Linglin Zhou, Yiling Wang, Tianci Hu, Xiao Qi, Fengyu Li, Feihong Huang, Wenchuan Peng, Xinyue Shen, Siyu Huang, Mengying Lei, Anguo Wu, Jianming Wu, Jiesi Luo, Long Wang, Artemisinin derived from *Artemisia annua* L. promotes thrombopoiesis *via* targeting FLT3: a novel strategy for thrombocytopenia management, Chinese Journal of Natural Medicines, 2026, 24(11), 1322−1342. doi: 10.1016/S1875−5364(26)61223−X.

View online: https://doi.org/10.1016/S1875−5364(26)61223−X

Related articles that may interest you

Artemdubinoids A−N: novel sesquiterpenoids with antihepatoma cytotoxicity from *Artemisia dubia*

Chinese Journal of Natural Medicines. 2023, 21(12), 902−915 https://doi.org/10.1016/S1875−5364(23)60441−8

Three new carabrane sesquiterpenoid derivatives from the whole plant of *Carpesium abrotanoides* L.

Chinese Journal of Natural Medicines. 2021, 19(11), 868−873 https://doi.org/10.1016/S1875−5364(21)60091−2

Chemical synthesis of a synthetically useful L−galactosaminuronic acid building block

Chinese Journal of Natural Medicines. 2022, 20(5), 387−392 https://doi.org/10.1016/S1875−5364(22)60149−3

β−Carboline alkaloids from the roots of *Peganum harmala* L.

Chinese Journal of Natural Medicines. 2024, 22(2), 171−177 https://doi.org/10.1016/S1875−5364(24)60583−2

Artemisia kruhsiana leaf extract induces autophagic cell death in human prostate cancer cells

Chinese Journal of Natural Medicines. 2021, 19(2), 134−142 https://doi.org/10.1016/S1875−5364(21)60014−6

Exosomes derived from Nr−CWS pretreated MSCs facilitate diabetic wound healing by promoting angiogenesis *via* the circIARS1/miR−4782−5p/VEGFA axis

Chinese Journal of Natural Medicines. 2023, 21(3), 172−184 https://doi.org/10.1016/S1875−5364(23)60419−4

Wechat

Chinese Journal of Natural Medicines 24 (2026) 1322-1342

Contents lists available at ScienceDirect

Chinese Journal of Natural Medicines

journal homepage: www.cjnmcpu.com/



Original article

Artemisinin derived from *Artemisia annua* L. promotes thrombopoiesis *via* targeting FLT3: a novel strategy for thrombocytopenia management

Xinyue Mei[a,Δ], Sheng Liu[a,Δ], Linglin Zhou[a], Yiling Wang[b], Tianci Hu[a], Xiao Qi[a], Fengyu Li[a], Feihong Huang[a], Wenchuan Peng[a], Xinyue Shen[c], Siyu Huang[a], Mengying Lei[a], Anguo Wu[a,*], Jianming Wu[a,d,e,*], Jiesi Luo[d,*], Long Wang[a,*]

[a] *Department of Pharmacology, School of Pharmacy, Southwest Medical University, Luzhou 646000, China*
[b] *Emei Rehabilitation and Nursing Center of Joint Logistics Support Force of PLA, Pharmaceutical and Equipment Department, Emeishan 614200, China*
[c] *School of Public Health, Southwest Medical University, Luzhou 646000, China*
[d] *School of Basic Medical Sciences, Southwest Medical University, Luzhou 646000, China*
[e] *Key Laboratory of Medical Electrophysiology, Sichuan Key Medical Laboratory of New Drug Discovery and Druggability Evaluation, Luzhou Key Laboratory of Activity Screening and Druggability Evaluation for Chinese Materia Medica, Southwest Medical University, Luzhou 646000, China*

ARTICLE INFO

Article history:
Received 1 February 2026
Revised 5 June 2026
Accepted 12 July 2026
Available online 20 November 2026

Keywords:
Artemisia annua L
Artemisinin
Megakaryocyte differentiation
Thrombocytopenia
FLT3

ABSTRACT

Artemisia annua L. (*A. annua*) has long been documented in traditional Chinese medicine for managing hemorrhagic conditions, attributed to its cooling and hemostatic properties. These historical applications suggest a potential role of *A. annua* in platelet-related disorders, although its hematopoietic mechanisms remain unclear. To investigate the thrombopoietic activity of *A. annua*, identify its bioactive constituent, and elucidate the molecular mechanisms underlying its effects on thrombopoiesis. Chemical profiling identified major compounds in *A. annua*. MK differentiation was assessed in K562, Meg-01 cells, and primary murine haematopoietic stem and progenitor cells (HSPCs). A murine radiation-induced thrombocytopenia (RIT) model was used to evaluate *in vivo* efficacy. Molecular docking, drug affinity responsive target stability (DARTS), and signaling assays were conducted to explore molecular mechanisms. *A. annua* promoted MK differentiation, upregulating CD41/CD42b and enhancing polyploidization. Artemisinin was identified as the principal active compound. It promoted MK maturation *in vitro* and restored platelet counts, MK numbers, and HSPC populations in RIT mice without inducing systemic toxicity. Artemisinin also reduced bone marrow (BM) apoptosis and DNA damage while restoring platelet function. Mechanistically, artemisinin directly bound to FLT3 and activated the FLT3/MAPK pathway, leading to increased phosphorylation of MEK/ERK and upregulation of NF-E2 and TAL1. FLT3 and ERK inhibition abrogated these effects. Artemisinin is a potent thrombopoietic agent that acts *via* direct activation of FLT3 and its downstream MAPK signaling cascade. The findings identify FLT3 as a novel therapeutic target for thrombocytopenia and support the potential clinical application of artemisinin in radiation-related hematological disorders.

1. Introduction

Ionizing radiation (IR), arising from therapeutic interventions, diagnostic exposures, or accidental nuclear events, exerts profound biological effects on multiple organ systems, with the hematopoietic compartment being especially susceptible [1]. The bone marrow (BM), as the central site of blood cell production, is highly vulnerable to radiation-induced damage, which disrupts hematopoietic stem and progenitor cell function [2, 3]. One of the most clinically significant consequences of this injury is thrombocytopenia—a reduction in circulating platelet counts—that can result in life-threatening hemorrhage and compromise the delivery of curative cancer treatments [4]. Despite the pressing clinical need, current therapeutic interventions for radiation-induced thrombocytopenia (RIT) remain inadequate. Agents such as thrombopoietin receptor agonists (TPO-RAs) offer some benefit but are limited by safety concerns and variable efficacy [5]. As such, there is a compelling need to explore novel pharmacological strategies that can restore platelet homeostasis through alternative, physiologically relevant mechanisms.

Platelets are essential cellular components of the circulatory system, primarily responsible for maintaining vascular integrity, mediating coagulation, and participating in inflammatory and immune responses [6]. These anucleate cytoplasmic fragments, known as platelets, originate from megakaryocytes (MKs)—large, polyploid cells that reside in the BM. Platelet production, or thrombopoiesis, is the culmination of a tightly regulated maturation program. This process begins with the differentiation of hematopoietic stem cells (HSCs) into megakaryocyte-erythroid

* Corresponding author.
E-mail addresses: wuanguo@swmu.edu.cn (A.Wu); jianmingwu@swmu.edu.cn (JM. Wu); ljs@swmu.edu.cn (JS. Luo); wanglong1226@swmu.edu.cn (L. Wang)
Δ These authors contributed equally to this work.

https://doi.org/10.1016/S1875-5364(26)61223-X
Copyright © 2026, China Pharmaceutical University. Published by Elsevier B.V. All rights are reserved.

progenitors (MEPs), followed by lineage commitment to MK progenitors. Subsequent stages include endomitosis, which leads to polyploidization, extensive cytoplasmic growth, and the development of an intricate demarcation membrane system (DMS). MKs then produce proplatelet projections into vascular sinusoids, where they are cleaved under shear stress to release circulating platelets [7]. The orchestration of MK development is governed by network of signaling pathways and transcriptional regulators. Key signaling cascades involved in this process include the thrombopoietin (TPO)/c-MPL, which activates downstream JAK2/STAT5, PI3K/Akt, and MAPK/ERK signaling to regulate proliferation and maturation of MKs [7, 8]. Additionally, BM microenvironment provides supportive cues through fibroblast growth factors (FGFs), interleukins (e.g., IL-6, IL-11), and chemokines such as chemokine ligand 5 (CCL5). At the transcriptional level, transcription factors such as NF-E2 and TAL1 coordinate gene expression critical for platelet biogenesis. Disruption of these regulatory networks can lead to defective thrombopoiesis and persistent thrombocytopenia [7, 9, 10].

Traditional Chinese medicine (TCM) has been extensively utilized in clinical practice for treating hematological disorders, and numerous herbal preparations have demonstrated therapeutic efficacy in managing cytopenias, particularly those secondary to chemotherapy or radiotherapy. Among these, botanicals with hematopoietic-promoting properties have attracted increasing attention due to their multi-targeted effects and favorable safety profiles [11-13]. *Artemisia annua* L. (*A. annua*), the dried aerial part of *Artemisia annua* L., is a well-known medicinal plant in the Asteraceae family, widely cultivated and utilized across various regions of China. It has traditionally been employed to clear internal heat, cool the blood and stop bleeding, relieve summer heat, and treat malaria, as well as for the management of inflammation and cardiovascular diseases. *A. annua* has long been recorded in classical texts for managing hemorrhagic disorders caused by "blood heat" or "deficiency heat." In the *Zhouhou Beiji Fang* (*Handbook of Prescriptions for Emergency*), fresh juice or poultices of *A. annua* were prescribed for traumatic bleeding, reflecting its cooling and hemostatic effects. Later texts, including the *Sheng Ji Zonglu* (*General Records of Holy Universal Relief*), documented its use in formulas for epistaxis and purpura. Modern practice has extended these applications, with compound *A. annua* preparations developed for bleeding management and reports of decoctions improving hemorrhagic symptoms and platelet counts in immune thrombocytopenic purpura [14-16]. Pharmacological studies further demonstrated pro-coagulant activity of *A. annua* extracts, supporting its potential in platelet-related disorders [17]. Phytochemical investigations have shown that *A. annua* contains a diverse spectrum of bioactive constituents, including sesquiterpenoids, diterpenoids, flavonoids, alkaloids, coumarins, lignans, and volatile oils [18-20]. Among these, sesquiterpene lactones—most notably artemisinin—are recognized as the principal pharmacologically active compounds. Although artemisinin is primarily known for its antimalarial efficacy, accumulating pharmacological evidence suggests that artemisinin and its derivatives possess additional bioactivities, including anti-inflammatory, antioxidant, antineoplastic, immunomodulatory, endocrine-regulating, and neuroprotective effects [21-23]. Despite these pleiotropic actions, the hematopoietic effects of *A. annua* and artemisinin, particularly their roles in thrombopoiesis, have not been systematically studied.

Here, we performed chemical characterization of *A. annua* and evaluated its ability to induce MK differentiation using established hematopoietic cell lines. Through activity screening, artemisinin was identified as the primary bioactive compound responsible for promoting MK differentiation. Subsequently, we investigated effects of artemisinin on MK differentiation and platelet production *in vitro* and *in vivo*. Furthermore, mechanistic studies were conducted to elucidate the target and signaling pathways involved in artemisinin-mediated thrombopoietic activity. Collectively, this work provides experimental evidence supporting the utility of artemisinin as a novel thrombopoietic agent.

2. Materials and methods

2.1. Chemicals

A. annua was obtained from Sichuan Neo-Green Pharmaceutical Technology Development Co., Ltd. Artemisinin (CAS: 63968-64-9) was purchased from Biopurify Phytochemicals Ltd. (Chengdu, China). Citrulline (CAS: 372-75-8) was purchased from Chengdu Must Bio-Technology Co., Ltd. (Chengdu, China). L-phenylalanine (CAS: 63-91-2) was purchased from Shanghai Macklin Biochemical Technology Co., Ltd. (Shanghai, China). Pantothenic acid (CAS: 79-83-4) was purchased from Shanghai Acmec Biochemical Technology Co., Ltd. (Shanghai, China). Apigenin (CAS: 520-36-5) was purchased from Chengdu Lemeitian Pharmaceutical Technology Co., Ltd. (Chengdu, China). (+)-Lariciresinol (CAS: 27003-73-2) was purchased from Shanghai YuanYe Biotechnology Co., Ltd. (Shanghai, China). Dihydroartemisinic acid (CAS: 85031-59-0) was purchased from Shanghai Macklin Biochemical Technology Co., Ltd. (Shanghai, China). gama-tocopherol (CAS: 54-28-4) was purchased from Shanghai Macklin Biochemical Technology Co., Ltd. (Shanghai, China).

2.2. Identification of constituents in A. annua

Fingerprint analysis of *A. annua* was perfomed using the Liquid Chromatography-Mass Spectrometry (LC-MS). LC analysis was performed on a Vanquish UHPLC System (Thermo Fisher Scientific, USA). Chromatography was achieved using an ACQUITY UPLC ® HSS T3 (Milford, MA, USA). The mobile phase was delivered at a flow rate of 0.3 $mL \cdot min^{-1}$, and the injection volume was 2 μL. Mass spectrometric analysis was performed on an Orbitrap Exploris 120 (Thermo Fisher Scientific, USA). Data acquisition was conducted in Full MS with data-dependent MS/MS mode, allowing for simultaneous collection of precursor and fragment ion spectra.

2.3. Cell culture

Meg-01 and K562 cells were propagated in RPMI-1640 supplemented with 10% fetal bovine serum and 1% penicillin–streptomycin. The cultures were kept under standard conditions at 37 °C with 5% CO_2 in a humidified environment.

2.4. Cell counting Kit-8

Cells were seeded and three parallel wells were set for each condition, including background, blank, and varying drug concentrations. On days 1, 3, and 5 after seeding, 20 μL of Cell Counting Kit-8 (CCK-8) solution (APExBIO, USA) was added. After incubation, absorbance was measured and cell proliferation rate was calculated.

2.5. Lactate dehydrogenase assay

Each group—including control, maximum lactate dehydrogenase (LDH) release, vehicle control, and various drug concentrations—was prepared in triplicate. On days 1, 3, and 5 post-seeding, 50 μL of complete medium was added to each well, followed by 50 μL of cell suspension. On the designated days, 20 μL of LDH release reagent (Beyotime, Shanghai, China) was added to

the maximum release group. After incubation, supernatants were collected, and the LDH activity was measured.

2.6. Giemsa staining

On day 5 after drug treatment, cells from 12-well plates were harvested and resuspended in 600 μL of 0.075 mol·L^{-1} KCl. The cell suspension was subsequently fixed for 5 min using a methanol–acetic acid mixture (3 : 1, *V/V*). Fixed samples were dispensed onto clean glass slides, air-dried, and immersed in Giemsa solution (Solarbio, Beijing, China), and finally examined under light microscope.

2.7. Phalloidin staining

On day 5 after drug treatment, cells were fixed with 4% paraformaldehyde, and transferred onto glass slides and air-dried. After permeabilization with 0.5% Triton X-100, samples were incubated with TRITC Phalloidin (Solarbio, Beijing, China) and DAPI. Images were acquired under an fluorescence microscope.

2.8. In vitro assessment of MK differentiation by flow cytometry

On day 5 after drug treatment, cells were collected. For Meg-01 and K562 cells, FITC-CD41 (Elabscience, Wuhan, China) and PE-CD42b (4A Biotech, Beijing, China) antibodies were added. For murine haematopoietic stem and progenitor cells (HSPCs), FITC-CD41 (Elabscience, Wuhan, China) and PerCP/Cyanine5.5-CD61 (BioLegend, San Diego, CA, USA) were used. Samples were incubated in the dark, then transferred to flow cytometry tubes for analysis using a flow cytometer.

2.9. DNA ploidy

On day 5 following drug treatment, cells were preserved in 70% chilled ethanol. After centrifugation, the cell pellet was incubated in pre-chilled PI and subsequently analyzed using a flow cytometer.

2.10. Network pharmacology analysis of A. annua against thrombocytopenia

The canonical SMILES notation for 21 compounds of *A. annua* was obtained from PubChem database. These SMILES strings were submitted to Swiss Target Prediction platform to predict potential protein targets. Predicted targets were subsequently standardized by UniProt database.

2.11. Targets prediction of A. annua against thrombocytopenia

Targets associated with thrombocytopenia were compiled from GeneCards, Online Mendelian Inheritance in Man (OMIM), and Therapeutic Target Database (TTD). Redundant entries were removed to obtain a unique set of disease-related targets. The intersecting targets between *A. annua*-predicted targets and thrombocytopenia-associated targets were identified using a Venn diagram tool.

2.12. Protein–protein interaction (PPI) network

Genes were uploaded to STRING database, applying confidence interaction score threshold of 0.900. Cytoscape 3.10.0 was used to visualized. An initial screening was performed to identify key targets, selecting nodes with degree values greater than 10. Subsequently, a more stringent filtering was applied to isolate core targets, defined as nodes with degree values exceeding 65. Both key and core target networks were iteratively visualized to highlight pivotal proteins within the interaction network.

2.13. Visualization of the A. annua compounds–Target–Thrombocytopenia network

A comprehensive network integrating 21 compounds of *A. annua*, potential targets, and thrombocytopenia-associated targets was constructed and visualized in Cytoscape 3.10.0. This network facilitated the identification of key molecular interactions and provided insight into the multi-target pharmacological profile of *A. annua*.

2.14. Gene Ontology (GO) and Kyoto Encyclopedia of Genes and Genomes (KEGG) pathway enrichment analysis

Targets were subjected to functional enrichment analysis using the DAVID bioinformatics resource. GO terms covering biological processes (BP), cellular components (CC), and molecular functions (MF), as well as KEGG pathway analyses, were conducted with a significance threshold of $P < 0.05$.

2.15. Network pharmacology of Artemisinin

First, putative targets of artemisinin were identified by retrieving its SMILES structure from the PubChem database and submitting it to the SwissTargetPrediction platform. In parallel, target data were also acquired from Traditional Chinese Medicine Systems Pharmacology Database (TCMSP).

Second, gene associated with MK differentiation were collected by querying the GeneCards database using the keyword "megakaryocyte differentiation". After removing duplicate entries, a comprehensive list of differentiation-related targets was compiled. Similarly, thrombocytopenia targets were curated from GeneCards, OMIM, and TTD platforms.

To identify overlapping targets between artemisinin, megakaryocyte differentiation, and disease-related gene sets, Venn diagrams were generated using Venn tool. Three sets of intersecting targets were defined.

Interaction analysis was conducted by STRING database. Nodes without any protein–protein interactions were excluded. The exported interaction datasets were visualized by Cytoscape 3.10.0. Targets with degree values greater than 45 were defined as key nodes, and subsequent filtering of nodes with degree values exceeding 74 was performed to identify core targets. These network subsets were visualized separately to highlight central nodes in the artemisinin-mediated thrombopoietic network.

Subsequently, a comprehensive Artemisinin–Target–Megakaryocyte differentiation–Thrombocytopenia interactive network was established in Cytoscape, integrating pharmacological targets and disease relevance. This visual network framework was used to explore the potential synergistic mechanisms by which artemisinin modulates thrombopoiesis.

Finally, GO and KEGG enrichment analyses were conducted by DAVID database. Significance threshold of $P < 0.05$ was applied.

2.16. Isolation and culture of HSPCs

BM cells were collected by flushing the marrow cavities with a 1 mL syringe using sterile buffer until the bones were visibly devoid of marrow. HSPCs were subsequently enriched from the collected BM cells through EasySep™ Mouse Haematopoietic Progenitor Cell Isolation Kit (STEMCELL Technologies, Vancouver, Canada), according to the manufacturer's protocol. The purified HSPCs were cultured in StemSpan™ serum-free expansion medium (STEMCELL Technologies, Vancouver, Canada) with cytokines including TPO (20 ng·mL^{-1}) and interleukin-3 (IL-3,

20 ng·mL^{-1}). After 72 hours' incubation, samples were treated with TPO (20 ng·mL^{-1}) and artemisinin (2.5, 5, and 10 μmol·L^{-1}) for 5 days to assess its effects on cell differentiation.

2.17. RIT model and artemisinin administration

Kunming mice (8–10 weeks old) were housed under standard conditions and randomly assigned to four groups (n = 8 per group; equal male-to-female ratio): untreated control, irradiated model, TPO-positive control, and artemisinin treatment groups. With the exception of the control group, all animals were subjected to a single 4 Gy total body irradiation (TBI) using an X-ray generator to establish a RIT model [24, 25]. Beginning on second day post-irradiation, model group received daily intraperitoneal injections of sterile saline. The positive control group received TPO at a dose of 3000 mg·kg^{-1}·d^{-1} (i.p.), while the treatment groups were administered artemisinin at 2.5, 5, or 10 mg·kg^{-1}·d^{-1} (i.p.). Drug administration continued for 17 consecutive days. Animals experiments were approved by the Laboratory Animal Ethics Committee of Southwest Medical University (Luzhou, China) and carried out in strict accordance with relevant ethical standards and institutional guidelines (Approval No.: 20240728-002).

2.18. Hematological analysis

Blood samples were obtained from retro-orbital sinus using capillary tubes on days 0, 3, 7, 10, 12, and 14 post-treatment. Blood parameters were measured by automated hematology analyzer.

2.19. Analysis of BM cells

BM cells were flushed from the femurs using 1 mL PBS. RBCs were lysed using RBC lysis buffer. The remaining cells were incubated with the following antibodies according to manufacturer instructions: FITC-CD34 (4A Biotech, Beijing, China), PE-c-Kit (Proteintech, Chicago, USA), FITC-CD41 (Elabscience, Wuhan, China), PerCP/Cyanine5.5-CD61 (BioLegend, San Diego, CA, USA), and PerCP/Cyanine5.5-CD42d (BioLegend, San Diego, CA, USA). Annexin V-FITC/PI Apoptosis Detection Kit (Vazyme, Nanjing, China) was used for apoptosis analysis. Cells were incubated with FITC-CD41 (Elabscience, Wuhan, China) and PI to assess DNA ploidy via flow cytometer.

2.20. Immunohistochemical staining

On day 10 after drug administration, bilateral femurs were collected, fixed, and decalcified. Samples were processed *via* routine dehydration, paraffin embedding, and sectioned. Immunohistochemical staining was performed sequentially, including endogenous peroxidase blocking, normal serum blocking, primary and secondary antibody incubation, DAB chromogenic reaction, hematoxylin counterstaining, and mounting. Primary antibodies used were: Bax and Caspase-3 (Servicebio, Wuhan, China), γ-H2AX (Abmart, Shanghai, China), and CD41 (Proteintech, Chicago, USA).

2.21. Organ coefficient analysis

On day 17 after treatment, major organs were excised and weighed. Organ coefficients were calculated as the ratio of organ weight to body weight.

2.22. Hematoxylin and eosin (H&E) staining

The organs were fixed in 4% paraformaldehyde. Femurs were decalcified prior to paraffin embedding. Tissue specimens were processed by paraffin embedding, sectioned, deparaffinized with xylene, and subjected to H&E staining. Stained samples were dried, mounted, and scanned through digital slide scanner.

2.23. Serum biochemical parameters

On day 17 after drug administration in irradiated mice, whole blood was collected via retro-orbital bleeding. Serum was isolated from blood. Serum levels of alanine aminotransferase (ALT), aspartate aminotransferase (AST), creatinine (CREA), urea (UREA), creatine kinase (CK), LDH, and glomerular filtration rate (GFR) were measured using an automated biochemical analyzer.

2.24. Tail bleeding time assay

On day 10 after drug administration, the distal 2 mm of the mouse tail was transected. The tail was immediately immersed in a beaker containing isotonic saline at room temperature. The time from the onset of bleeding to complete cessation was recorded. If bleeding persisted beyond 10 min, bleeding duration was noted to exceed 10 min [24, 25].

2.25. Whole blood clot retraction assay

On day 10 after drug administration in irradiated mice, whole blood was collected *via* retro-orbital bleeding. Blood samples were immediately transferred into siliconized, flat-bottom glass tubes pre-rinsed with serum. Each tube was supplemented with normal saline, whole blood, and 1 U·mL^{-1} thrombin (Solarbio, Beijing, China). Samples were treated for 1 h. Images of clot were captured at 0 and 60 min. After incubation, the weight of the formed clot was measured using an electronic balance [26].

2.26. Molecular docking simulations

Three-dimensional structure of FLT3 was obtained from AlphaFold. Protonation state of the small-molecule compounds was adjusted to physiological pH (7.4), and their three-dimensional conformations were generated using Open Babel. Receptor and ligand preparation, including the addition of polar hydrogens and assignment of Gasteiger charges, was performed using AutoDock Tools (ADT 1.5.7). The docking grid box was defined using AutoGrid based on the predicted active site of FLT3. Docking was conducted by AutoDock Vina (version 1.2.0), and the top-ranked binding pose based on binding affinity used for subsequent analysis. Interactions were visualized and analyzed using PyMOL (version 2.5.4) [25].

2.27. Molecular dynamics simulations

Desmond/Maestro noncommercial version 2022.1 was used. System was solvated with explicit TIP3P water molecules and neutralized with 0.15 mol·L^{-1} sodium chloride to simulate physiological conditions. After system energy minimization and equilibration, a 100-nanosecond molecular dynamics production run was carried out under constant temperature and pressure conditions (300 K and 1 bar). Snapshots of system were saved every 100 ps throughout the simulation. Post-simulation analyses were conducted via Simulation Interaction Diagram from Desmond [25].

2.28. Drug affinity responsive target stability assay (DARTS)

K562 cells were lysed by ice-cold RIPA buffer (CST, MA, USA) supplemented with protease inhibitors. Lysates were centrifuged at 4 °C, and the supernatants were collected and equally divided into two aliquots. One was treated with artemisinin (final concen-

tration, 20 μmol·L^{-1}), and the other with an equal volume of DMSO. Pronase was added at dilutions of 1 ∶ 500, 1 ∶ 1000, and 1 ∶ 1500, followed by incubation at 40 °C for 10 min. The mixtures were incubated at 70 °C for 10 min to facilitate protein denaturation, and immediately snap-frozen at −20 °C. Protein samples were loaded based on the post-digestion volume and analyzed by SDS-PAGE [25,26].

2.29. siRNA transfection

FLT3 knockdown was performed using small interfering RNA (siRNA). Briefly, each siRNA was dissolved in 125 μL nuclease-free water to prepare a 20 μmol·L^{-1} stock solution. For each transfection, 2.5 μL siRNA stock solution was mixed with 2.5 μL siRNA-Mate SUS 2X Buffer to obtain a 5 μL mixture. Subsequently, 5 μL siRNA-Mate SUS Reagent (GenePharma, Shanghai, China) was added, gently mixed by pipetting, and incubated at room temperature for 5 min to form a 10 μL siRNA transfection complex. The transfection complex was then added to 1 mL complete medium containing 5 × 10^5 cells. Cells were incubated at 37 °C in a humidified atmosphere containing 5% CO_2. FLT3 protein expression was examined at 72 h after transfection, and MK differentiation was evaluated on day 4.

The siRNA sequences were as follows: negative control siRNA (NC), 5′-UUCUCC GAACGUGUCACGUTT-3′; siFLT3-1, 5′-GGACUAUUACAAAUCAAGATT-3′; siFLT3-2, 5′-GGUGCUGUGCCAGAAAUGATT-3′; and siFLT3-3, 5′-GGUGCA AAGCUGUUCAUGUTT-3′.

2.30. Western blot

Experimental methods were referenced from previously published studies [25,26]. Primary antibodies used: GAPDH (Proteintech, Chicago, USA), FLT3 (Abcam, Cambridge, UK), RAS (Abcam, Cambridge, UK), p-MEK (Abcam, Cambridge, UK), MEK (Abcam, Cambridge, UK), p-ERK (Abcam, Cambridge, UK), ERK (Abcam, Cambridge, UK), NF-E2 (Proteintech, Chicago, USA), TAL-1 (Abmart, Shanghai, China), c-Fos (Proteintech, Chicago, USA), and c-Jun (Proteintech, Chicago, USA).

2.31. Statistical analysis

Data are presented as mean ± standard deviation (SD) from at least three independent experiments. Student's *t*-test was used for comparisons between two groups. For comparisons among multiple groups, one-way analysis of variance (ANOVA) followed by Tukey's multiple comparison test was performed. For data involving two independent variables, such as treatment and time, two-way ANOVA followed by Tukey's multiple comparison test was used. A value of $P < 0.05$ was considered statistically significant.

3. Results

3.1. Characterization of ingredients of A. annua

To elucidate the phytochemical profile of *Artemisia annua* L. and provide a basis for subsequent pharmacological evaluation, its chemical constituents were analyzed using high-performance LC-MS. Total ion chromatograms were obtained under both positive and negative ionization conditions, enabling broad coverage of the compound profile (Fig. S1). Based on preliminary analysis of the MS data, a total of 22 representative compounds were tentatively identified (Table. 1). The corresponding chemical structures of these compounds are presented in Fig. 1. These identified constituents provide a chemical basis for subsequent pharmacological investigations.

3.2. A. annua promotes MK differentiation in vitro

To evaluate hematopoietic potential of *A. annua*, we investigated its effects on Meg-01 and K562 cells, commonly used to study MK development. First, the effect of *A. annua* on cell proliferation was detected. The results showed that treatment with *A. annua* (6.25, 12.5, 25, and 50 μg·mL^{-1}) for 1, 3, and 5 days had no significant impact on the proliferation of two cell lines (Figs. 2A and 2C). To determine whether *A. annua* exerted cytotoxic effects, lactate dehydrogenase (LDH) release assays were performed. No significant differences in LDH between *A. annua*-treated cells and controls in two cell lines, indicating *A. annua* does not induce cytotoxicity under these experimental conditions (Figs. 2B and 2D). We next examined the morphological changes induced by *A. annua* treatment. PMA (8 nmol·L^{-1}) is a positive control. After 5 days of exposure, microscopy revealed an increased presence of enlarged cells in both Meg-01 and K562 cultures compared to controls, suggestive of MK differentiation (Fig. 2E). Giemsa staining further confirmed this observation, showing increased cell size, nuclear enlargement, and nuclear lobulation—morphological hallmarks of maturing MKs (Fig. 2F). Similarly, phalloidin staining indicated cytoskeletal reorganization associated with cell enlargement and increased nuclear content in both cell lines following *A. annua* treatment (Fig. 2G). To further confirm MK differentiation, CD41 and CD42b expression was assessed. *A. annua* significantly upregulated both markers in Meg-01 and K562 cells relative to controls, supporting its role in inducing MK lineage commitment (Figs. 2H, 2J and 2L). As MK maturation is characterized by endomitosis and DNA polyploidization, we conducted ploidy analysis by flow cytometry. *A. annua* treatment markedly increased the proportion of cells with 4N DNA content in both cell lines, indicating enhanced polyploidization and progression toward terminal MK maturation (Figs. 2I, 2K and 2M). The results demonstrate that *A. annua* effectively promotes MK differentiation.

3.3. Identification of molecular mechanisms involved in A. annua's therapeutic action against thrombocytopenia

Network pharmacology approach was employed to illuminate the potential action mechanisms of *A. annua* on thrombocytopenia. A number of 1301 putative targets were identified for 21 compounds of *A. annua*. Meanwhile, 6405 thrombocytopenia-related genes were obtained from multiple databases. The intersection of these datasets yielded 561 common targets, suggesting potential relevance of *A. annua* to thrombocytopenia pathophysiology. A PPI network was constructed based on the 561 overlapping targets (Fig. 3A). Network topology analysis was subsequently conducted in Cytoscape. Key targets were identified as nodes with degree values greater than 10, resulting in 129 key targets. Further filtration revealed 46 core targets with degree values exceeding 65, indicating their central roles in the interaction network (Figs. 3B–3D). To explore the pharmacological landscape of *A. annua* in the context of thrombocytopenia, a compound–target–disease network was constructed, integrating all 21 compounds, the 46 core targets, and thrombocytopenia-related targets (Fig. 3E). This network highlighted the multi-component, multi-target nature of *A. annua*, providing insights into its systemic regulatory potential.

Functional enrichment analyses were then conducted on the 46 core targets. GO enrichment revealed significant involvement in BP such as phosphatidylinositol 3-kinase activator activity, as well as CC including cytoplasm, nucleus, and caveola. For MF, these targets were enriched in pathways related to positive regulation of ERK1 and ERK2 cascade, and MAPK cascade (Fig. 3F).

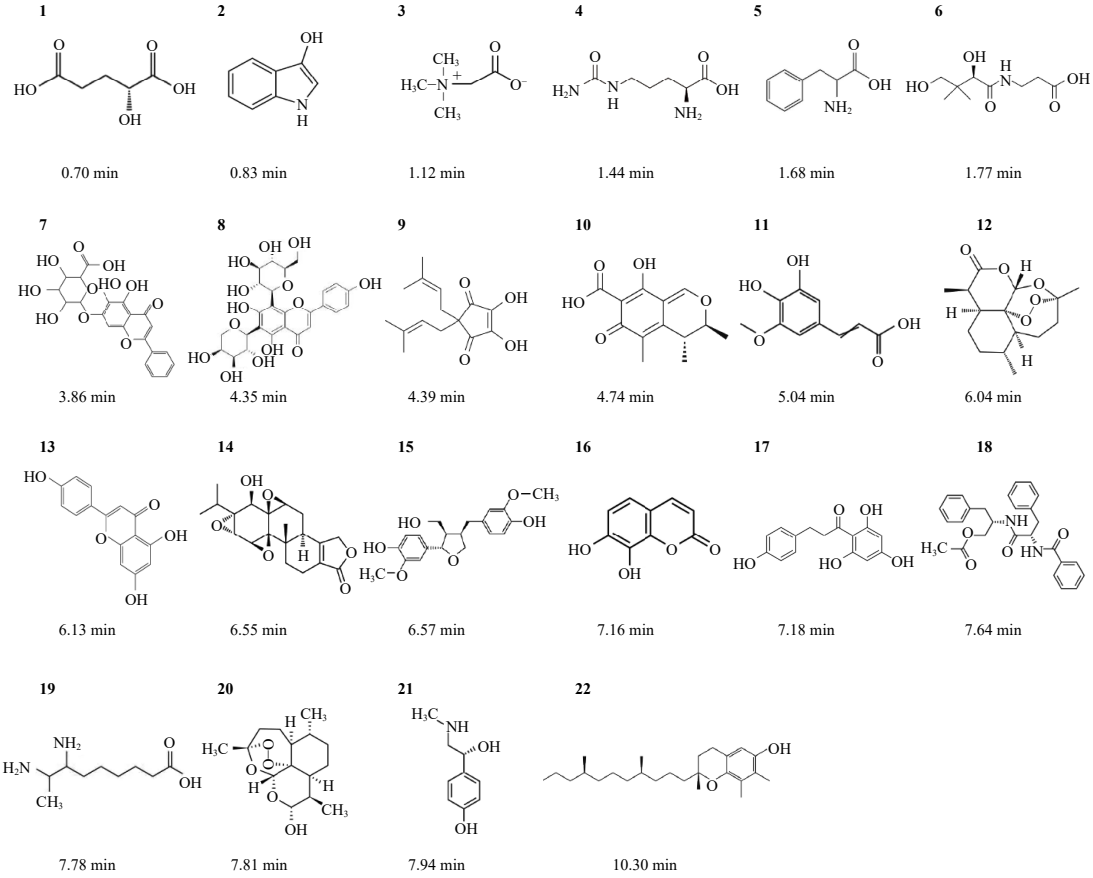


Fig. 1 Characterization of compounds in *A. annua*. (A) Total ion chromatogram in positive ion mode. (B) Total ion chromatogram in negative ion mode. (C) Chemical structures of representative identified constituents in *A. annua*.

These processes are closely associated with MK proliferation, differentiation, and platelet biogenesis [7, 27]. KEGG pathway analysis further showed that core targets were involved in pathways known to regulate hematopoiesis and thrombopoiesis, including the PI3K-Akt, HIF-1, MAPK, Estrogen, Ras, JAK-STAT, Toll-like receptor signaling pathways, Platelet activation, and Hematopoietic cell lineage. Notably, several of these pathways such as PI3K-Akt and MAPK are well-characterized downstream effectors of TPO/c-MPL signaling, and are essential for promoting MK maturation and platelet production [7] (Fig. 3G).

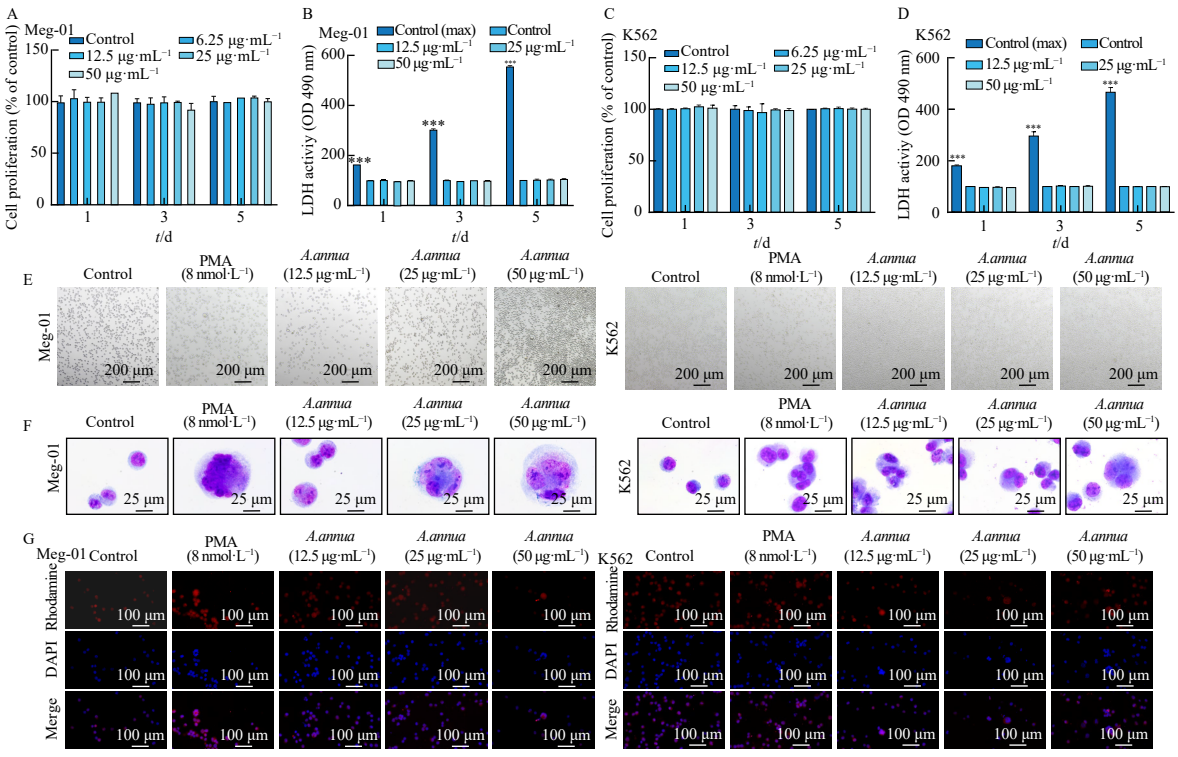
Overall, these findings suggest that *A. annua* exerts its therapeutic effect against thrombocytopenia through coordinated modulation of multiple signaling pathways implicated in MK differentiation and thrombopoiesis. The integration of key molecular targets and regulatory nodes highlights the multi-target pharmacological characteristics of *A. annua* and supports its potential as a promising candidate for thrombocytopenia intervention.

3.4. Artemisinin acts as the principal active compound in A. annua responsible for inducing MK differentiation

To identify the key bioactive constituent responsible for the MK-promoting activity of *A. annua*, we performed a bioactivity-guided screening of its major components. Eight representative constituents identified from *A. annua*, including citrulline, L-phenylalanine, pantothenic acid, artemisinin, apigenin, (+)-lariciresinol, dihydroartemisinic acid, and gamma-tocopherol, were individually tested in K562 cells. MK differentiation was evaluated by flow cytometric analysis of CD41 and CD42b expression. Among the tested components, artemisinin exhibited the strongest activity, markedly increasing the proportion of $CD41^{+}CD42b^{+}$ cells compared with the control group, whereas the other compounds showed no obvious or only limited effects under the same screening conditions (Fig. S1). These findings suggested that artemisinin may be the principal active constituent contributing to the MK differentiation-promoting effect of *A. annua*. To further validate the biological activity of artemisinin, we first assessed its impact on cell proliferation and found that treatment with artemisinin for 5 days promoted cell proliferation in Meg-01 cells at concentrations of 2.5, 5, 10, and 20 μmol·L^{-1} (Fig. 4A). In contrast, artemisinin at concentrations of 1.25, 2.5, 5, 10, and 20 μmol·L^{-1} had no significant effect (Fig. 4C). To evaluate potential cytotoxicity, LDH release assays were conducted, which revealed no significant difference between groups, indicating a lack of overt cytotoxic effects (Figs. 4B and 4D). Subsequently, giemsa staining and phalloidin staining were employed to assess changes in cell morphology and nuclear content. Artemisinin (2.5, 5, and 10 μmol·L^{-1}) treatment led to a pronounced increase in cell size and nuclear number, both of which are characteristic features of MK differentiation and maturation (Figs. 4F and 4G). In addition, flow cytometric analysis revealed that artemisinin enhanced the CD41/CD42b expressions in two cell lines, further confirming its capacity to drive MK differentiation (Figs. 4H, 4J and 4L). Moreover, artemisinin elevated 4N and 8N cells in Meg-01 and K562 cells, indicating enhanced polyploidization—a hallmark of mature MKs (Figs. 4I, 4K and 4M). To determine whether artemisinin accounts for its megakaryopoietic activity, we performed parallel experiments using primary haematopoietic stem and progenitor cells (HSPCs) isolated from murine BM. Cells were first cultured with TPO and IL-3 to initiate differentiation, followed by treatment with TPO (20 ng·mL^{-1}) and artemisinin for 5 days. Morphological evaluation revealed a notable increase in cell size in artemisinin-treated cultures (Fig. 4N). Giemsa staining demonstrated enhanced nuclear size and increased nuclear lobulation, indicative of progressing MK maturation (Fig. 4O). A dose-dependent elevation in $CD41^{+}CD61^{+}$ cells, and a concomitant in-

Table 1 The compounds of *A. annua*.

No.	Identity	Mode	Molecular formula	RT (t/min)	$[M + H]^+$ (m/z)
1	D-2-hydroxyglutaric acid	neg	$C_5H_8O_5$	0.70	148.03717
2	Indoxyl	pos	C_8H_7NO	0.83	133.0527612
3	Trimethylglycine	pos	$C_5H_{11}NO_2$	1.12	117.07897
4	Citrulline	pos	$C_6H_{13}N_3O_3$	1.44	175.09569
5	L-phenylalanine	pos	$C_9H_{11}NO_2$	1.68	165.07897
6	Pantothenic acid	pos	$C_9H_{17}NO_5$	1.77	219.11067
7	Baicalin	neg	$C_{21}H_{18}O_{11}$	3.86	446.08491
8	Isoshaftoside	pos	$C_{26}H_{28}O_{14}$	4.35	564.1479
9	Hulupinic acid	neg	$C_{15}H_{20}O_4$	4.39	264.13615
10	Citrinin	neg	$C_{13}H_{14}O_5$	4.74	250.08412
11	5-hydroxyferulic acid	pos	$C_{10}H_{10}O_5$	5.04	210.052821
12	Artemisinin	pos	$C_{15}H_{22}O_5$	6.04	282.14672
13	Apigenin	neg	$C_{15}H_{10}O_5$	6.13	270.05282
14	Triptolide	pos	$C_{20}H_{24}O_6$	6.55	360.15728
15	(+)-lariciresinol	neg	$C_{20}H_{24}O_6$	6.57	360.15728
16	7,8-dhmc	pos	$C_{10}H_8O_4$	7.16	192.04226
17	Phloretin	neg	$C_{15}H_{14}O_5$	7.18	274.08412
18	Aurantiamide acetate	pos	$C_{27}H_{28}N_2O_4$	7.64	444.2049
19	7,8-diaminopelargonate	neg	$C_9H_{20}N_2O_2$	7.78	188.15247
20	Dihydroartemisinic	pos	$C_{15}H_{24}O_2$	7.81	236.17762
21	P-synephrine	pos	$C_9H_{13}NO_2$	7.94	167.09462
22	Gamma-tocopherol	neg	$C_{28}H_{48}O_2$	10.30	416.36541



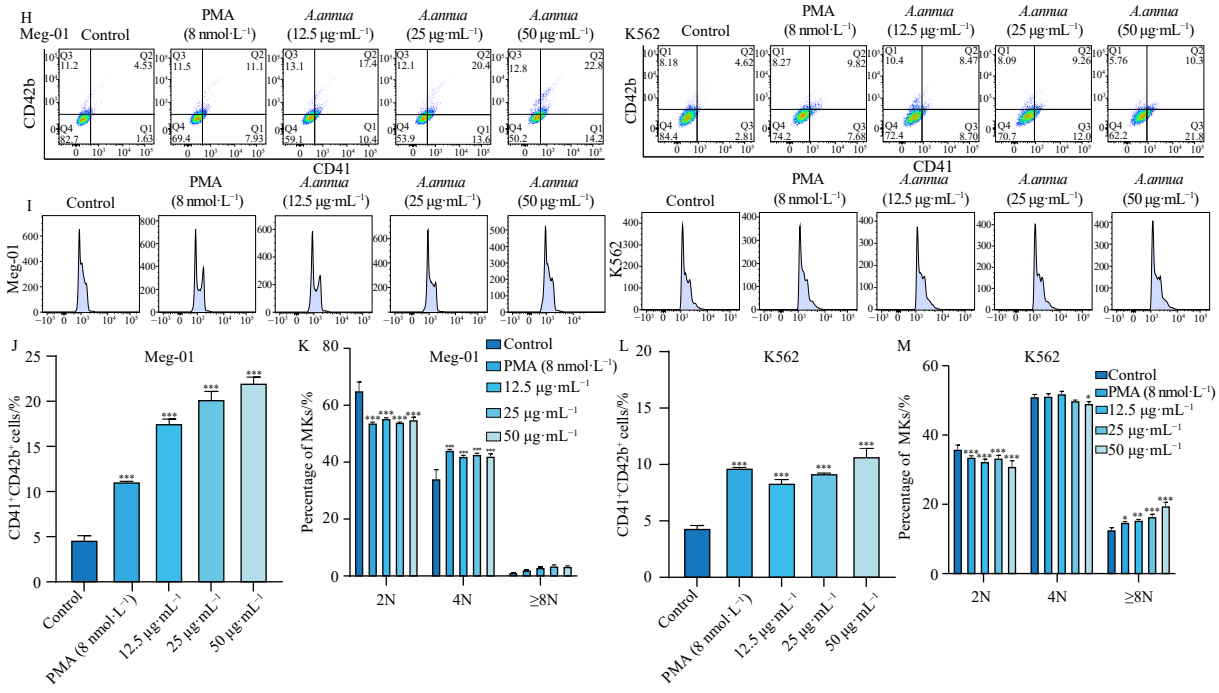


Fig. 2 Effects of *A. annua* on MK differentiation *in vitro*. (A) Cell proliferation of Meg-01 cells treated with *A. annua* (6.25, 12.5, 25, and 50 μg·mL^{-1}) for 1, 3, and 5 days, assessed by CCK-8 assay (n = 3). (B) LDH release in Meg-01 cells following exposure to *A. annua* (12.5, 25, and 50 μg·mL^{-1}) for 1, 3, and 5 days (n = 3). (C) Cell proliferation of K562 cells treated with *A. annua* (6.25, 12.5, 25, and 50 μg·mL^{-1}) for 1, 3, and 5 days (n = 3). (D) LDH release in K562 cells after treatment with *A. annua* (12.5, 25, and 50 μg·mL^{-1}) for 1, 3, and 5 days (n = 3). (E) Morphological changes in Meg-01 and K562 cells observed by bright-field microscopy after 5 days of treatment with *A. annua* (12.5, 25, and 50 μg·mL^{-1}) or PMA (8 nmol·L^{-1}). Scale bar = 200 μm. (F) Giemsa staining of Meg-01 and K562 cells following the same treatments to assess nuclear morphology. Scale bar = 25 μm. (G) Cytoskeletal organization visualized by phalloidin staining after 5-day treatment. Scale bar = 100 μm. (H) Expression of CD41 and CD42b in Meg-01 and K562 cells evaluated by flow cytometry after 5-day exposure. (I) DNA ploidy distribution analyzed by flow cytometry in both cell lines following treatment. (J–M) Quantitative analysis of CD41$^+$CD42b$^+$ cell populations (J for Meg-01; L for K562) and polyploid cells (K for Meg-01; M for K562) after 5-day treatment (n = 3). Data are presented as mean ± SD. Statistical significance was determined using one-way ANOVA. $^*P < 0.05$, $^{**}P < 0.01$, $^{***}P < 0.001$ *vs* corresponding Control group.

crease in CD41$^+$CD61$^+$ platelet-like particles were observed, suggesting that artemisinin effectively promotes both MK differentiation and platelet generation in primary hematopoietic cells (Figs. 4Q–4T). The findings suggest that artemisinin robustly induces MK differentiation and maturation *in vitro*, not only in established cell lines but also in primary murine HSPCs. These findings confirm that artemisinin is the principal active compound within A. annua responsible for its thrombopoietic efficacy.

3.5. Artemisinin alleviates radiation-induced hematopoietic injury in RIT mice

The therapeutic potential of artemisinin was assessed in RIT mice (Fig. 5A). Compared with the untreated RIT model group, TPO-treated group exhibited significantly less severe declines in platelet levels at this time point. From day 10 onward, platelet counts gradually recovered. On days 10, 12, and 14 post-treatment, platelet levels in treatment groups were higher than irradiated mice. By day 17, platelet counts in the artemisinin group had returned to baseline physiological levels, whereas the TPO group exhibited supraphysiological platelet levels, consistent with the known clinical side effect of thrombocytosis associated with TPO therapy. These results demonstrate that artemisinin effectively accelerates platelet recovery following irradiation without inducing excessive platelet elevation (Fig. 5B). Notably, artemisinin treatment did not significantly affect mean platelet volume (MPV) (Fig. 5E). In addition to its effects on platelet regeneration, artemisinin also promoted recovery of other hematological parameters. White blood cell (WBC) counts markedly declined on the day of irradiation but gradually increased thereafter. Artemisinin administration (10 mg·kg^{-1}) significantly improved WBC recovery on days 10 and 12 post-treatment (Fig. 5C). A similar effect in red blood cell (RBC) counts was observed, where artemisinin treatment enhanced RBC levels on day 10, indicating its broader hematopoietic protective effects (Fig. 5D).

To investigate whether artemisinin mitigates radiation-induced BM apoptosis, flow cytometric analysis of apoptotic BM cells was performed. The results revealed that artemisinin significantly suppressed the increase in apoptosis triggered by irradiation (Fig. 5F). Immunohistochemical staining further demonstrated that artemisinin markedly downregulated the expression of Bax and Caspase-3 (Figs. 5G–5H). Given the known association between radiation exposure and DNA damage, we next assessed the expression of γ-H2AX in BM tissues. Immunohistochemical analysis showed that artemisinin reduced γ-H2AX expression levels, suggesting that it alleviates radiation-induced DNA damage in hematopoietic cells (Fig. 5I). To evaluate the systemic safety of artemisinin *in vivo*, body weights were monitored. Artemisinin-treated mice did not show body weight loss compared to irradiated mice (Fig. 6A). Organ coefficient analysis revealed no notable differences in the weight indices of heart, liver, spleen, lungs, kidneys, and thymus (Fig. 6B). Histopathological examination (H&E staining) of these organs revealed no overt structural abnormalities in artemisinin-treated mice (Fig. 6D). Moreover, serum biochemical parameters, including ALT, AST, CREA, UREA, CK, LDH, and GFR, remained within normal ranges and were unaffected by artemisinin treatment (Fig. 6C). Collectively, these findings indicate that artemisinin effectively ameliorates radiation-induced hematopoietic injury, promotes the recovery of multiple blood cell lineages, inhibits BM apoptosis and DNA damage, and exhibits no detectable systemic toxicity *in vivo*.

3.6. Artemisinin restores MK differentiation and platelet functionality in RIT mice

To determine whether observed increase in platelet level induced by artemisinin treatment is attributable to enhanced megakaryopoiesis, we examined the BM and spleen of RIT mice. Histo-

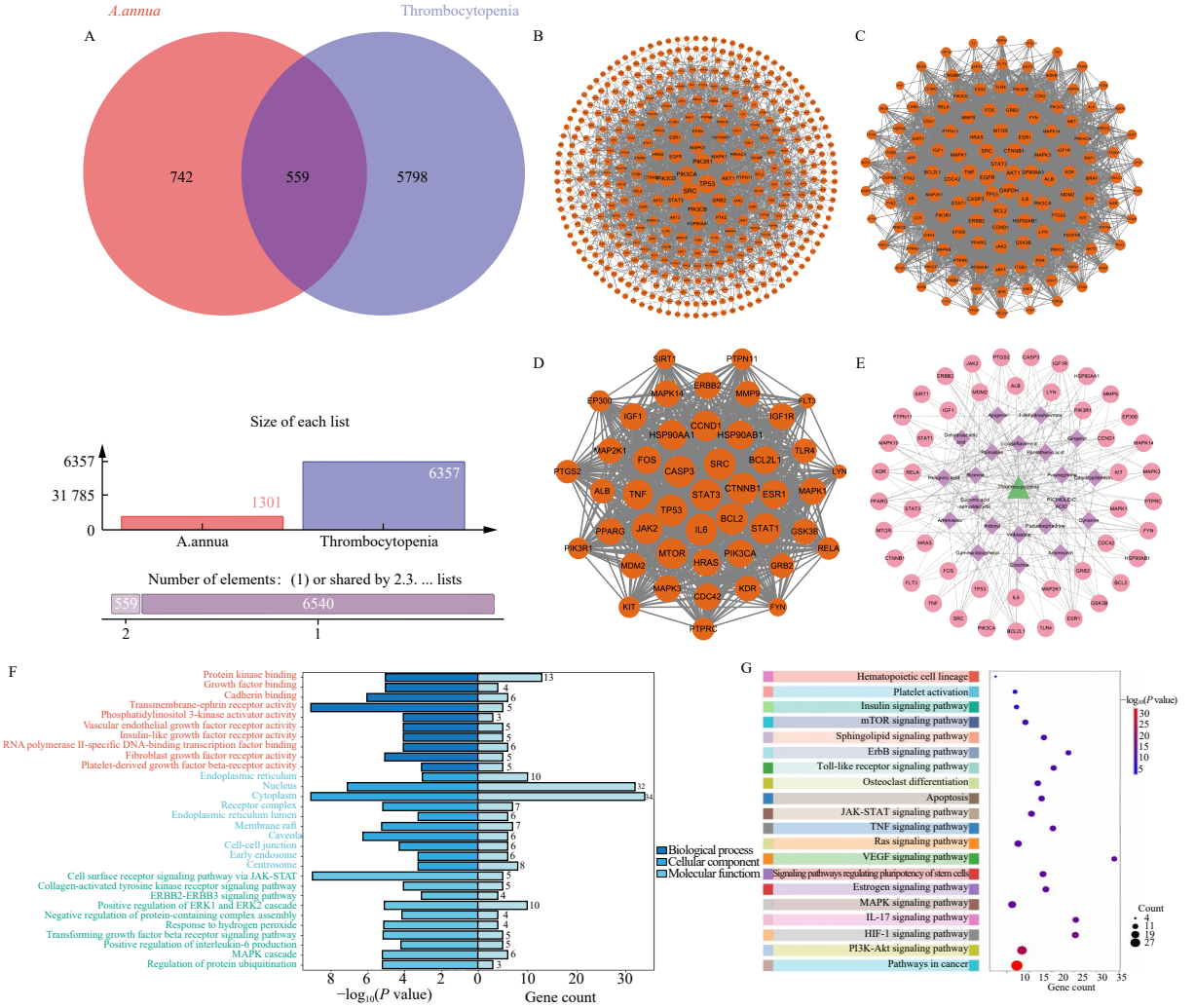
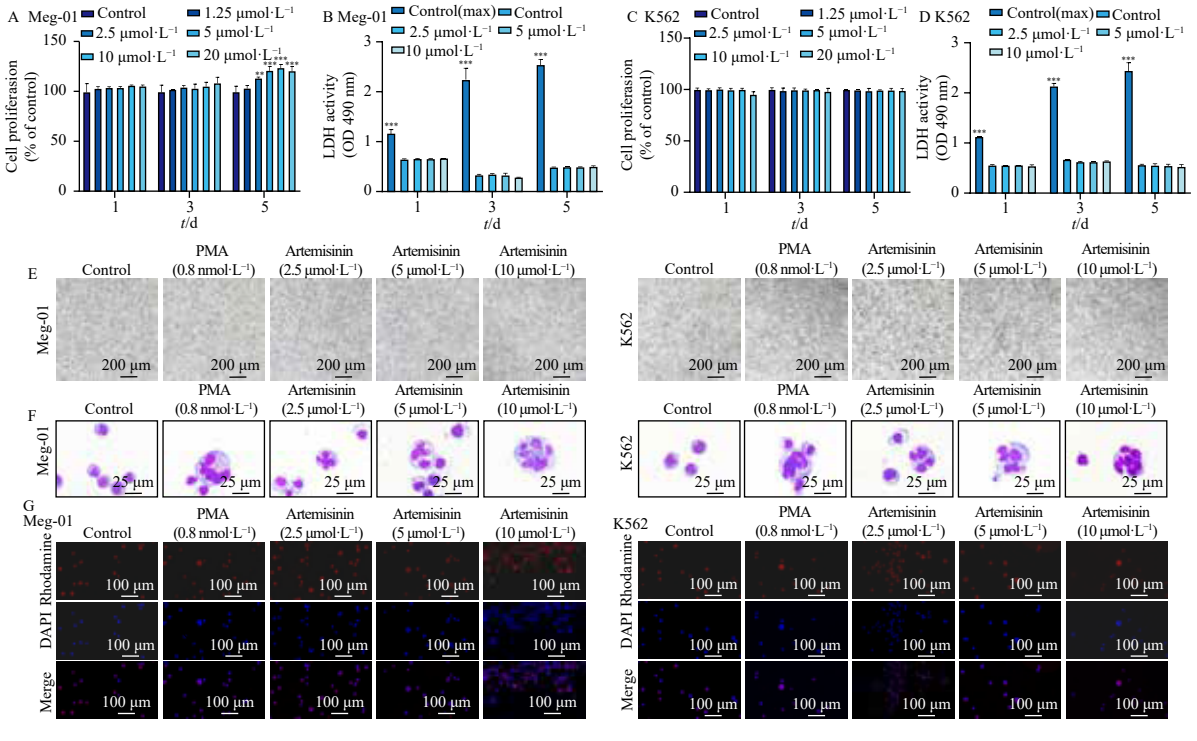


Fig. 3 Network pharmacology-based analysis of *A. annua* in thrombocytopenia. (A) Venn diagram illustrating the overlapping targets between *A. annua* compounds and thrombocytopenia-related genes. (B–D) PPI network of the targets. (E) Integrated compound–core target–disease network. (F) GO enrichment analysis of core targets. (G) KEGG pathway enrichment analysis of core targets.



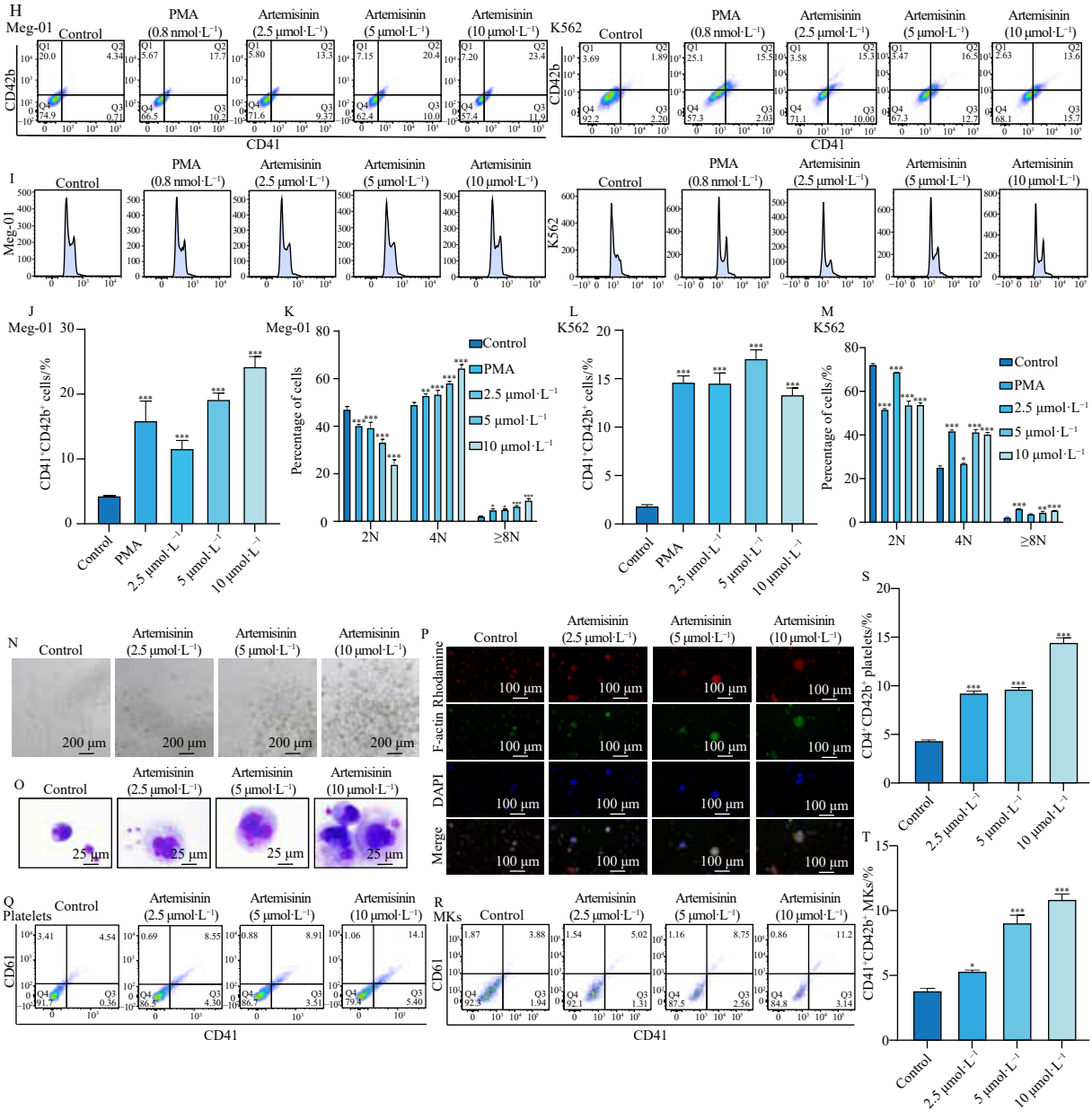


Fig. 4 Artemisinin promotes MK differentiation and platelet production *in vitro*. (A) Proliferation of Meg-01 cells treated with artemisinin (1.25, 2.5, 5, 10, and 20 μmol·L^{-1}) for 1, 3, and 5 days as assessed by CCK-8 assay (n = 3). (B) LDH release in Meg-01 cells following artemisinin treatment (2.5, 5, and 10 μmol·L^{-1}) for 1, 3, and 5 days (n = 3). (C) Proliferation of K562 cells after exposure to artemisinin (1.25, 2.5, 5, 10, and 20 μmol·L^{-1}) for 1, 3, and 5 days (n = 3). (D) LDH release in K562 cells treated with artemisinin (2.5, 5, and 10 μmol·L^{-1}) for 1, 3, and 5 days (n = 3). (E) Light microscopy images showing morphological changes in Meg-01 and K562 cells after 5-day treatment with artemisinin (2.5, 5, and 10 μmol·L^{-1}) or PMA (8 nmol·L^{-1}). Scale bar = 200 μm. (F) Giemsa staining of Meg-01 and K562 cells after 5-day treatment to evaluate nuclear morphology and lobulation. Scale bar = 25 μm. (G) Cytoskeletal remodeling visualized by phalloidin staining in Meg-01 and K562 cells following 5-day exposure. Scale bar = 100 μm. (H) Flow cytometric analysis of CD41 and CD42b expression in Meg-01 and K562 cells after 5-day treatment. (I) DNA ploidy analysis of Meg-01 and K562 cells assessed by flow cytometry following treatment. (J–M) Quantitative analysis of CD41$^+$CD42b$^+$ cells (J for Meg-01; L for K562) and polyploid cells (K for Meg-01; M for K562) (n = 3). (N) Morphological changes in murine HSPCs observed by light microscopy after 5 days of treatment with artemisinin (2.5, 5, and 10 μmol·L^{-1}). Scale bar = 200 μm. (O) Giemsa staining of HSPCs to assess nuclear size and morphology following artemisinin treatment. Scale bar = 25 μm. (P) Co-immunofluorescence staining of HSPCs using phalloidin and β-tubulin to examine cytoskeletal and nuclear structural alterations. Scale bar = 100 μm. (Q) Flow cytometric analysis of CD41$^+$CD42b$^+$ MKs derived from HSPCs after artemisinin treatment. (R) Flow cytometric detection of CD41$^+$CD61$^+$ platelets in artemisinin-treated HSPCs. (S–T) Quantification of CD41$^+$CD61$^+$ platelets (S) and CD41$^+$CD61$^+$ MKs (T) in HSPCs after 5-day exposure to artemisinin (n = 3). Data are presented as mean ± SD. Statistical significance was determined using one-way ANOVA. $^*P$< 0.05, $^{**}P$ < 0.01, $^{***}P$ < 0.001 *vs* corresponding Control group.

logical analysis of femoral BM sections by H&E staining revealed a significant reduction in MK numbers following irradiation, which was markedly reversed upon treatment with TPO or artemisinin (Fig. 7A). Immunohistochemical staining further confirmed an increased CD41$^+$ MKs of artemisinin-treated mice, indicating restoration of MK production (Fig. 7C). Given that the spleen serves as a secondary hematopoietic organ, we also assessed splenic megakaryopoiesis. H&E staining showed an increase in MK counts in spleens of artemisinin group, suggesting that extramedullary hematopoiesis may also contribute to the enhanced platelet production (Fig. 7B).

To investigate whether this increase in MK output was driven by expansion or differentiation of upstream progenitors, we assessed HSPC populations by flow cytometry. The frequency of CD34$^+$c-Kit$^+$ cells, representing HSPCs, was significantly decreased following irradiation but was restored upon treatment with either TPO or artemisinin (Fig. 7D). Furthermore, portion of c-Kit$^+$CD41$^+$ megakaryocytic progenitor cells was also reduced in irradiated mice and rescued by artemisinin administration, suggesting that artemisinin promotes the differentiation of HSPCs toward the megakaryocytic lineage (Fig. 7E). To directly assess MK differentiation and maturation, we evaluated the expression of

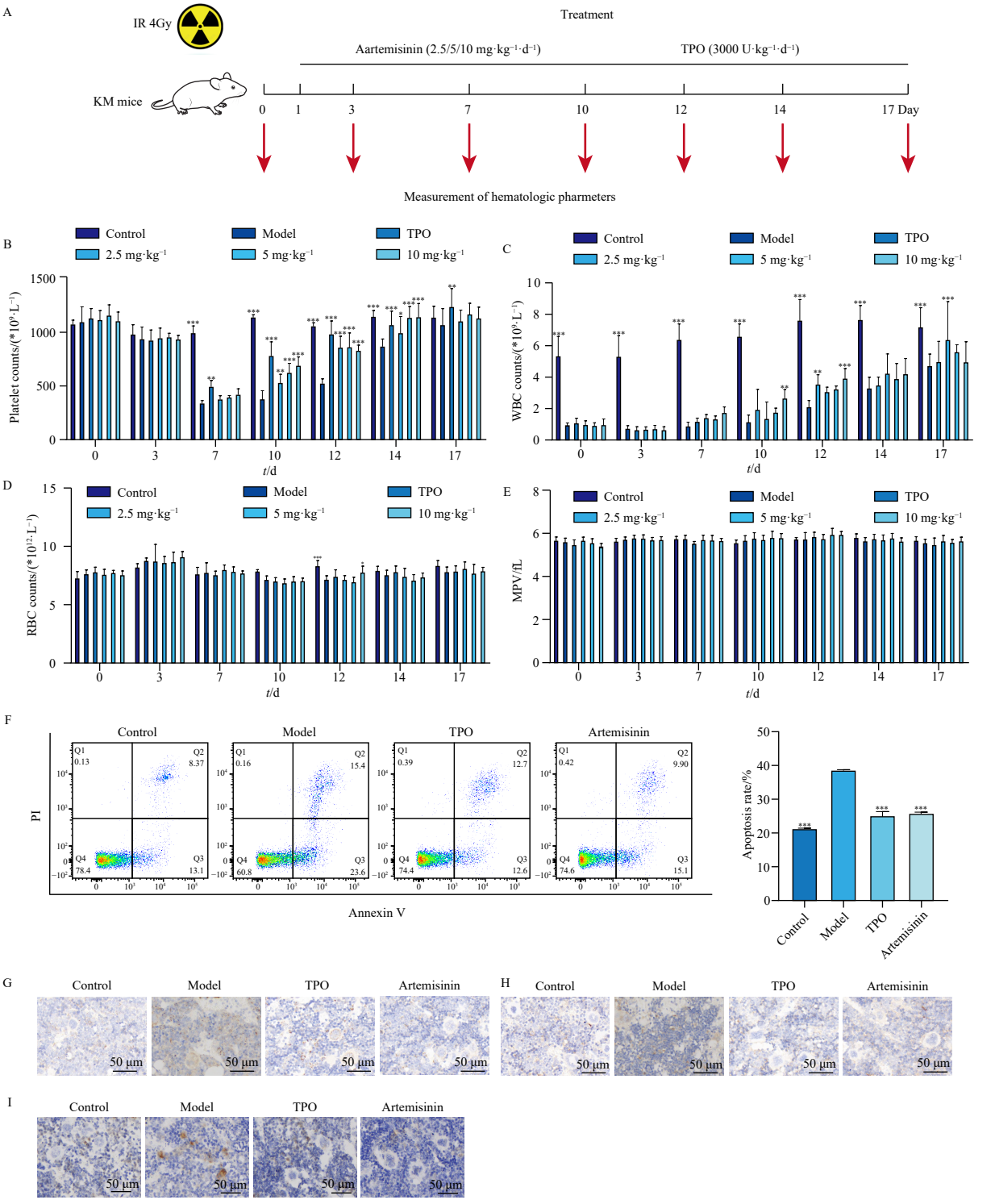


Fig. 5 Artemisinin facilitates hematopoietic recovery and mitigates radiation-induced injury in RIT mice. (A) Schematic diagram of the RIT model and artemisinin treatment regimen. (B–E) Time-course analysis of peripheral blood parameters including platelet counts (B), WBC counts (C), RBC counts (D), and MPV (E) in control, model, TPO-treated (3000 U·kg^{-1}), and artemisinin-treated (2.5, 5, and 10 mg·kg^{-1}) mice on days 0, 3, 7, 10, 12, 14, and 17 post-treatment (n = 8). (F) Flow cytometric analysis of apoptotic BM cells on day 10 post-treatment (n = 3). (G–I) Immunohistochemical staining of BM sections for pro-apoptotic proteins Bax (G) and Caspase-3 (H), and the DNA damage marker γ-H2AX (I) across all experimental groups. Scale bar = 50 μm. Data are presented as mean ± SD. For B–E, statistical significance was determined using two-way ANOVA; for F, one-way ANOVA was used. $^{*}P < 0.05$, $^{**}P < 0.01$, $^{***}P < 0.001$ *vs* Model group.

MK-specific surface markers in BM cells. Artemisinin increased proportion of CD41^{+}CD42d^{+} and CD41^{+}CD61^{+} cells, consistent with enhanced MK differentiation (Figs. 7F–7G). In addition, DNA ploidy analysis revealed that the percentages of 4N and 8N MKs were significantly elevated in artemisinin-treated mice, indicating that artemisinin promotes MK polyploidization and maturation, mirroring the effects observed *in vitro* (Fig. 7H). Finally, to examine platelet production, we measured the proportion of circulating reticulated platelets (CD41^{+}Thiazole Orange (TO)$^{+}$), which represent newly released platelets from the BM (Fig. 7I). Artemisinin significantly increased the frequency of reticulated platelets in the peripheral blood of RIT mice, further supporting its role in enhancing thrombopoiesis. To further determine whether artemisinin-induced platelets possess normal hemostatic functionality, several *in vitro* assays were conducted. Tail bleeding time, an indicator of primary hemostasis, was signific-

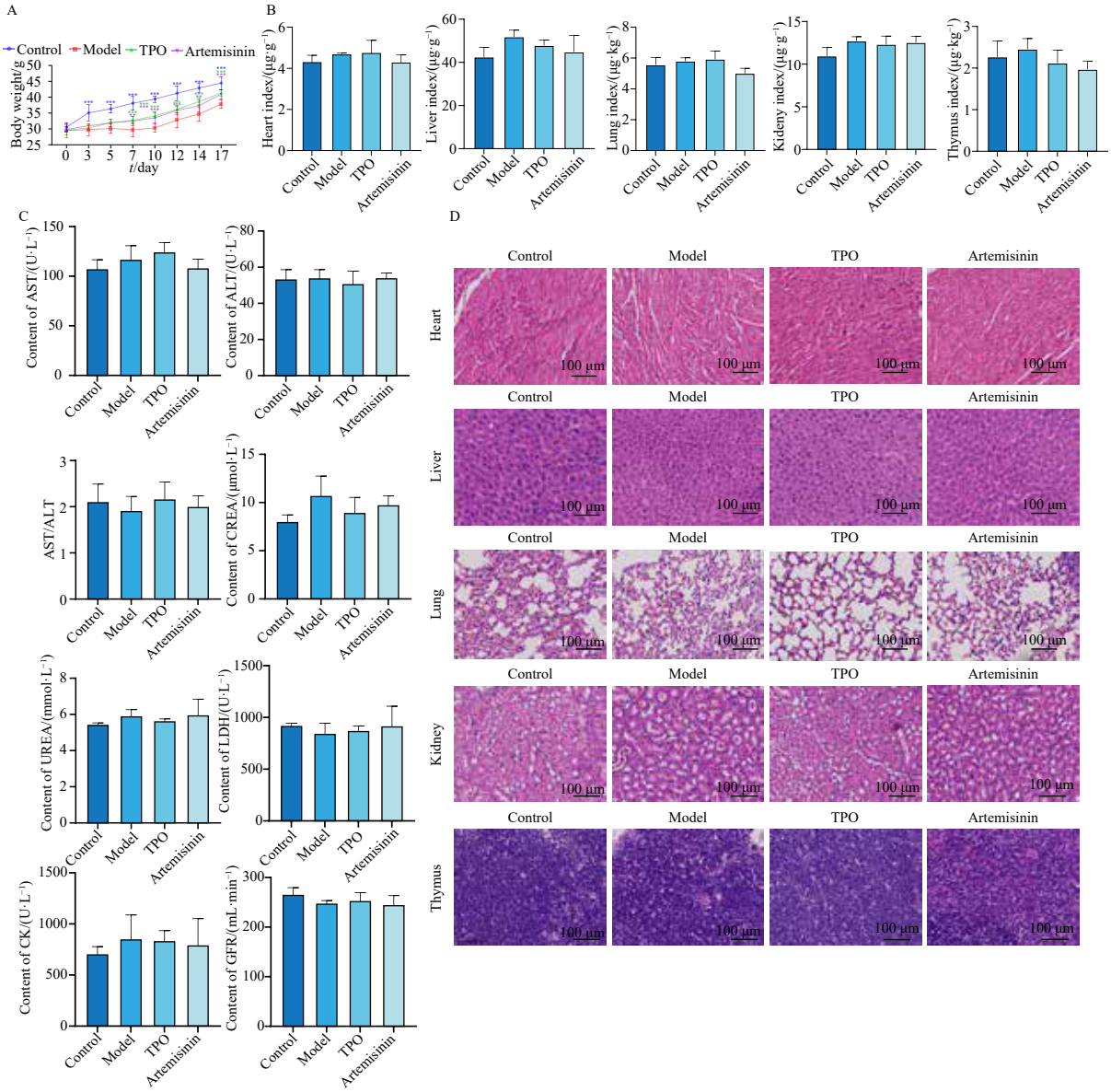


Fig. 6 Evaluation of the safety profile of artemisinin in RIT mice. (A) Body weight changes over the 17-day treatment period in each group (n = 8). (B) Organ indices of the heart, liver, lung, kidney, and thymus on day 17 (n = 3). (C) Serum biochemical parameters including AST, ALT, AST/ALT ratio, UREA, LDH, CK, and GFR in each group (n = 3). (D) Representative H&E staining of major organs (heart, liver, lung, kidney, thymus) on day 17. Scale bar = 100 μm. Data are presented as mean ± SD. For A, statistical significance was determined using two-way ANOVA, $^{**}P< 0.01$, $^{***}P < 0.001$ *vs* Model group; for B and C, one-way ANOVA was used, no significant difference was detected ($P > 0.05$) *vs* Model group.

antly prolonged in irradiated mice compared with healthy controls. Treatment with either TPO or artemisinin markedly shortened bleeding time in irradiated mice, indicating improved platelet-mediated hemostatic capacity (Fig. 7J). To assess the mechanical contractile function of platelets, whole blood clot retraction and purified platelet clot retraction assays were performed. The results demonstrated that TPO and artemisinin significantly enhanced clot retraction in both whole blood and platelet-rich conditions (Figs. 7K–7L). This suggests that artemisinin effectively restores the contractile function of platelets impaired by radiation injury. Taken together, these findings confirm that artemisinin not only restores HSPC populations and promotes their differentiation into megakaryocytic progenitors and mature MKs, but also enhances thrombopoiesis and facilitates the production of functionally competent platelets in a RIT model.

3.7. Elucidation of artemisinin targets involved in MK differentiation and thrombocytopenia

Building upon the *in vivo* evidence demonstrating that artemisinin promotes MK differentiation and alleviates thrombocytopenia, network pharmacology was employed to uncover its molecular mechanisms. A total of 198 artemisinin-associated targets were identified after integration and standardization of data from multiple prediction platforms. Concurrently, 6405 thrombocytopenia-related genes and 3964 MK differentiation-related targets were collected from disease and functional databases. Cross-referencing these three datasets revealed 123 overlapping genes, which may represent candidate targets through which artemisinin regulates MK differentiation to alleviate thrombocytopenia (Fig. 8A). To further dissect the functional relevance of these overlapping targets, a PPI network was constructed. Network topology analysis identified 70 key targets with degree values>45, among which 27 core targets were distinguished based on a higher connectivity threshold (degree > 74), suggesting their central role in the artemisinin-mediated regulatory axis (Figs. 8B–8D). A composite PPI map was then constructed to integrate these targets with MK differentiation and thrombocytopenia, revealing a densely interconnected subnetwork indicative of potential synergistic mechanisms (Fig. 8E).

GO analysis of 27 core targets demonstrated significant enrichment in BP such ad protein-containing complex binding (Fig. 8F). CC analysis revealed prominent localization in the cytosol, extracellular region, and nucleoplasm, supporting their involvement in dynamic intracellular signaling events. Key MF indicated a potential link between stress response, cell fate regulation, and MK maturation. KEGG pathway analysis further demonstrated that the core targets were predominantly related in signaling cascades directly implicated in hematopoiesis, including MAPK signaling pathway, Ras signaling pathway, and Hematopoietic cell lineage (Fig. 8G). These pathways are well recognized for their roles in orchestrating progenitor proliferation, MK differentiation, and platelet release [7, 9]. Overall, the findings suggest that artemisinin exert thrombopoietic functions through engaging key signaling pathways that govern MK lineage commitment and differentiation.

3.8. Artemisinin promotes MK differentiation through direct interaction with FLT3

To elucidate the direct molecular target through which artemisinin regulates MK differentiation, molecular docking simulations were employed to predict potential binding interactions between artemisinin with its core targets. The docking results revealed that artemisinin binds with high affinity to FLT3 (Fig. 9A), a class III receptor tyrosine kinase implicated hematopoiesis [25, 28, 29]. Specifically, the amino acid residue ARG170 was found to form a stable hydrogen bond with artemisinin (Fig. 9A), playing a critical role in stabilizing the protein–ligand complex. Additional hydrophobic and polar interactions involving neighboring residues contributed to the specificity and stability of the binding conformation (Fig. 9A). The estimated binding free energy of the artemisinin–FLT3 complex was −8.2 kcal·mol^{-1} (Fig. 9A), suggesting a strong and favorable interaction. To further characterize the dynamic stability of the artemisinin–FLT3 complex, molecular dynamics simulations were conducted. The root mean square deviation (RMSD) of the FLT3 backbone stabilized at approximately 4.0 Å following initial equilibration, while the ligand (artemisinin) maintained a relatively stable RMSD between 0.5 and 1.5 Å (Figs. 9B–9D), indicating limited conformational fluctuation and a high degree of structural compatibility. The root mean square fluctuation (RMSF) values for the binding site residues and the ligand atoms remained low throughout the simulation (Figs. 9B–9D), further supporting the stability of the complex. Importantly, ARG170 exhibited a hydrogen bond occupancy rate of 99% during the simulation (Figs. 9E and 9F), underscoring its key role in mediating ligand binding. Additional hydrogen bonds and water-bridged interactions were also observed (Figs. 9E and 9F), collectively enhancing the binding strength and structural integrity of the complex. These results suggest that the initial docking pose was further optimized through dynamic conformational adjustments, leading to a more stable and biologically relevant interaction model between artemisinin and FLT3. To experimentally validate this interaction, DARTS assay was performed. Treatment of K562 cells with artemisinin markedly stabilized FLT3 protein levels against protease-mediated degradation (Fig. 9G), confirming a direct physical interaction between artemisinin and FLT3 in cellular conditions. To assess whether artemisinin promotes MK differentiation *via* FLT3 activation, K562 cells were co-treated with artemisinin and the selective FLT3 inhibitor dovitinib (0.8 μmol·L^{-1}). Giemsa staining revealed a reduction of large, differentiated cells in combination group compared to artemisin-

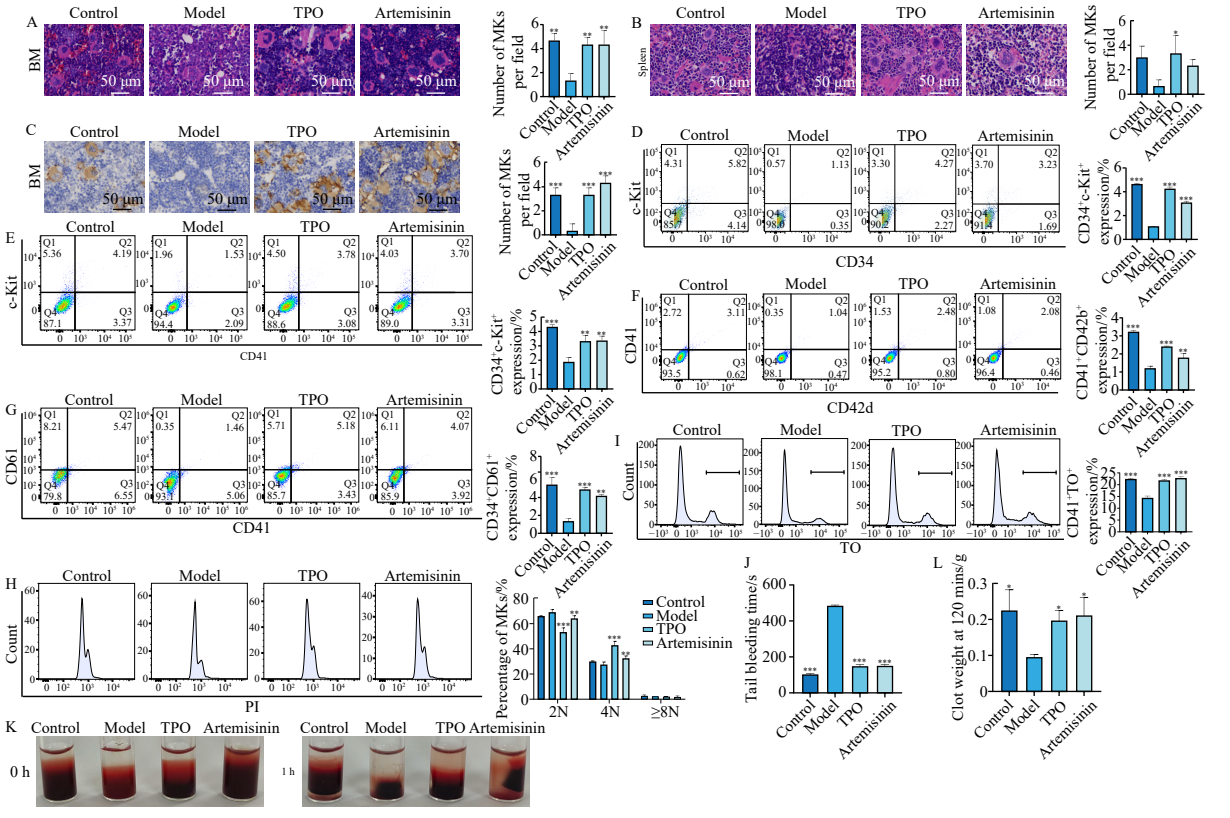


Fig. 7 Artemisinin promotes megakaryopoiesis and restores platelet production and function in irradiated mice. (A) Representative H&E staining of BM sections in each group (n = 3). Scale bar = 50 μm. (B) H&E staining of spleen sections in each group (n = 3). Scale bar = 50 μm. (C) Immunohistochemical staining of CD41$^+$ MKs in BM sections (n = 3). Scale bar = 50 μm. (D) Flow cytometry analysis of CD34$^+$c-Kit$^+$ cells in BM (n = 3). (E) Quantification of c-Kit$^+$CD41$^+$ cells in BM (n = 3). (F) Flow cytometry analysis of CD41$^+$CD42d$^+$ MKs in BM (n = 3). (G) Analysis of CD41$^+$CD61$^+$ MKs in BM (n = 3). (H) DNA ploidy analysis of BM MKs (n = 3). (I) Thiazole orange staining of circulating reticulated platelets in each group (n = 3). (J) Tail bleeding time measurements in each group (n = 3). (K) Representative images of clot retraction after 1 hour in each group. (L) Clot retraction assays in each group (n = 3). Data are presented as mean ± SD. Statistical significance was determined using one-way ANOVA. $^*P < 0.05$, $^{**}P < 0.01$, $^{***}P < 0.001$ *vs* Model group.

in treatment alone (Fig. 9H). Consistently, flow cytometric analysis showed that co-treatment with dovitinib markedly suppressed artemisinin-induced upregulation of CD41 and CD42b (Fig. 9I).

To further strengthen the functional evidence for FLT3 involvement, we performed siRNA-mediated FLT3 knockdown experiments in K562 cells. Three siRNAs targeting FLT3 were tested, and western blot analysis showed that siFLT3-2 and siFLT3-3 markedly reduced FLT3 protein expression compared with the NC, whereas siFLT3-1 showed only a limited knockdown effect (Fig. 10A). Therefore, siFLT3-2 and siFLT3-3 were selected for subsequent functional validation. We then evaluated whether FLT3 knockdown affected artemisinin-induced MK differentiation. Morphological observation showed that artemisinin treatment increased the number of enlarged megakaryocyte-like cells in the NC + artemisinin group, whereas this effect was clearly weakened in the artemisinin + siFLT3-2 and artemisinin + siFLT3-3 groups (Fig. 10B). Consistently, Giemsa staining showed that artemisinin induced typical megakaryocytic morphological features, including cell enlargement and nuclear enlargement, while these changes were attenuated after FLT3 knockdown Fig. 10C). Flow cytometric analysis was then performed to quantitatively assess MK differentiation. The results showed that artemisinin markedly increased the proportion of $CD41^{+}CD42b^{+}$ cells in the NC + artemisinin group, but this increase was substantially reduced after FLT3 knockdown (Fig. 10D). These data provide direct genetic evidence supporting the functional involvement of FLT3 in artemisinin-induced MK differentiation. Taken together, these findings demonstrate that artemisinin facilitates MK differentiation by directly binding to and modulating FLT3 activity.

3.9. Artemisinin promotes MK differentiation through FLT3-mediated activation of the MAPK signaling

We examined artemisinin's effect on the MAPK signaling cascade—identified via network pharmacology analysis as a key regulatory axis in artemisinin-mediated thrombopoietic activity. Results showed that artemisinin upregulated RAS expression and enhanced phosphorylation of MEK and ERK in K562 cells (Fig. 11A). In addition, we assessed the expression of downstream hematopoietic transcription factors. Artemisinin upregulated NF-E2, TAL1, c-Fos, and c-Jun expressions (Fig. 11A), all of which are critically involved in megakaryopoiesis.

To verify whether MAPK activation is required for artemisinin-induced MK differentiation and transcription factor upregulation, K562 cells were co-treated with artemisinin and the selective ERK inhibitor SCH772984. Giemsa staining revealed that co-treatment showed reduced enlarged, differentiated cells compared to artemisinin alone (Fig. 11B). Flow cytometry further showed that SCH772984 abrogated the artemisinin-induced upregulation of CD41 and CD42b (Fig. 11C). Western blot analysis confirmed that SCH772984 inhibited ERK phosphorylation and

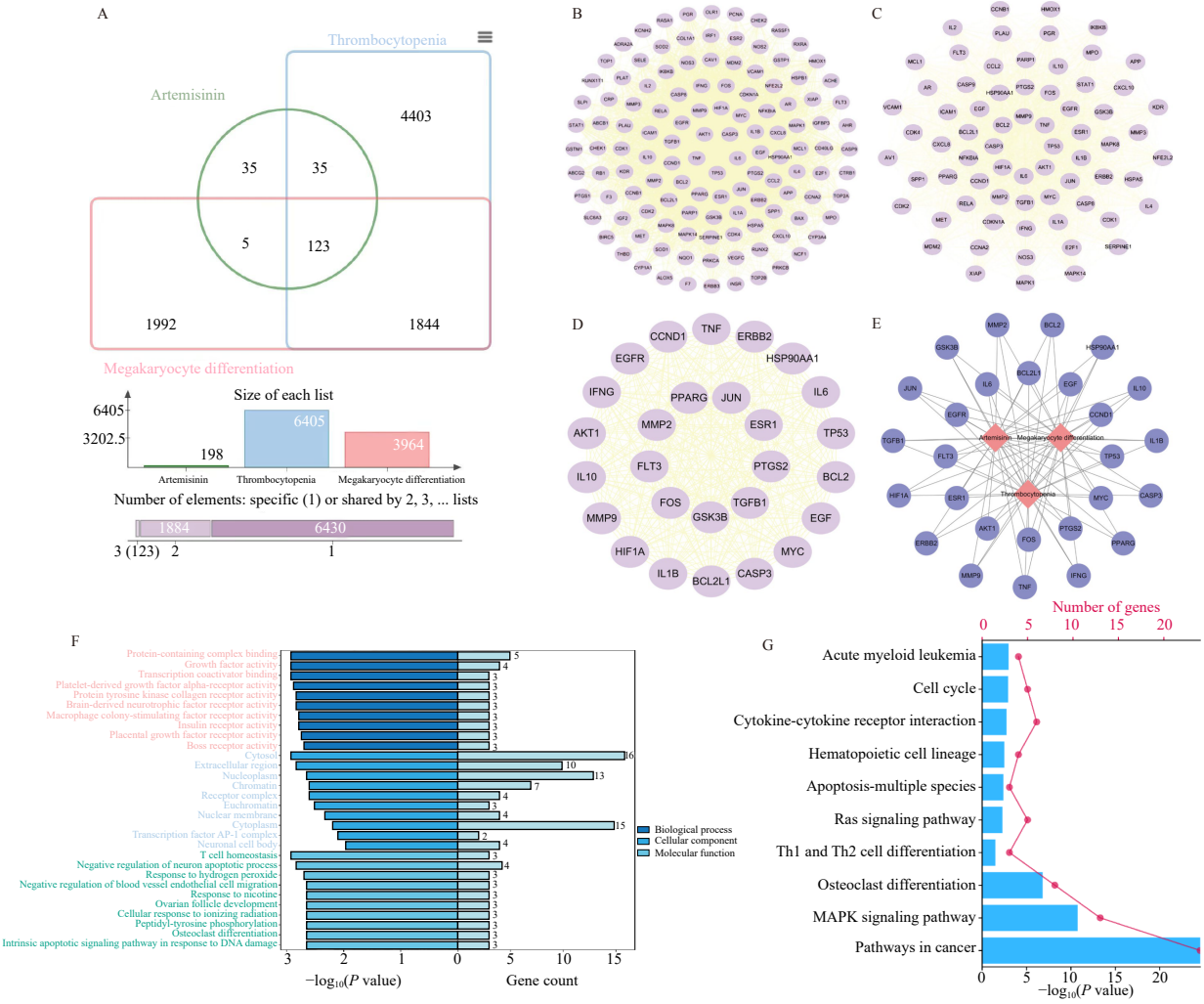


Fig. 8 Network pharmacology-based analysis of artemisinin in MK differentiation and thrombocytopenia. (A) Venn diagram illustrating the overlapping targets between artemisinin, MK differentiation and thrombocytopenia-related genes. (B-D) PPI network of the targets. (E) Integrated artemisinin–core target–MK differentiation–thrombocytopenia network. (F) GO enrichment analysis of core targets. (G) KEGG pathway enrichment analysis of core targets.

suppressed the artemisinin-mediated induction of NF-E2 and TAL1 expression (Fig. 11E). To determine the relationship between FLT3 and MAPK signaling, we examined the effect of FLT3 inhibition using dovitinib. Treatment with dovitinib markedly attenuated the artemisinin-induced MEK and ERK phosphorylation, as well as NF-E2 and TAL1 expressions (Fig. 11D), indicating that FLT3 acts upstream of the MAPK pathway in this context. Taken together, these findings demonstrate that artemisinin promotes MK differentiation by directly targeting FLT3, which in turn activates the MAPK signaling cascade and its downstream hematopoietic transcription factors, thereby driving the differentiation and maturation of MKs (Fig. 12).

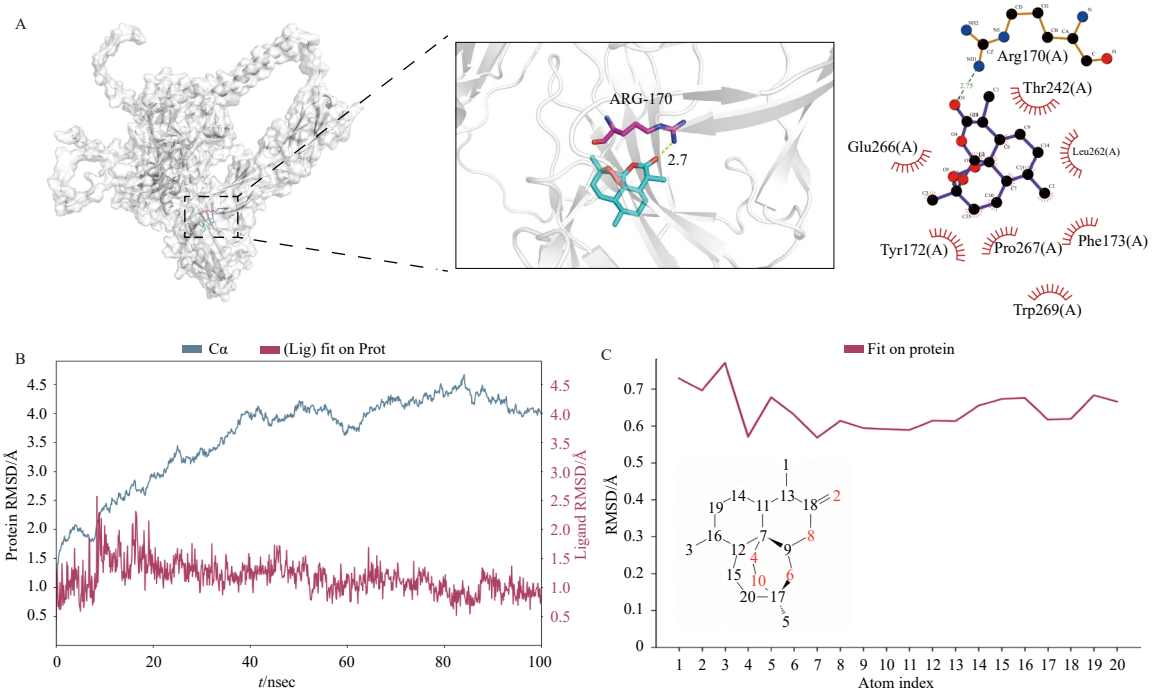
4. Discussion

IR poses a significant threat to hematopoietic homeostasis due to its profound cytotoxic effects on BM cellular components, particularly HSPCs. Among the hematological sequelae induced by IR, thrombocytopenia is one of the most clinically challenging complications, manifesting as a critical reduction in circulating platelet counts that compromises hemostatic capacity and increases hemorrhagic risk [1, 5]. In oncological settings, RIT often limits the intensity and continuity of radiotherapy regimens, thereby impacting treatment efficacy and patient prognosis [30, 31]. Current standard-of-care pharmacotherapies for RIT, such as TPO-RAs, including romiplostim and eltrombopag, have demonstrated efficacy in certain patient populations; however, their clinical application is constrained by adverse effects, including hepatotoxicity, thrombosis, and BM fibrosis, as well as variable response rates [32-34]. These limitations underscore the urgent need for novel thrombopoietic agents that not only possess robust efficacy but also offer a superior safety profile and target alternative regulatory mechanisms of megakaryopoiesis.

TCM represents a valuable resource for drug discovery, particularly in hematological disorders. Numerous botanical extracts have demonstrated efficacy in promoting hematopoiesis with minimal systemic toxicity, offering promising adjunct or alternative therapeutic options [11-13, 35]. Previous work from our group has demonstrated that aqueous extracts of herbs such as *Cibotii rhizoma* and *Caulis Polygoni Multiflori* significantly promote MK differentiation and accelerate platelet recovery in RIT models through modulation of key signaling cascades including PI3K/Akt, MAPK, and JAK2/STAT3 [13]. These findings provide a pharmacological rationale for exploring other medicinal plants traditionally used in TCM. *A. annua*, a widely distributed species in China, has traditionally been used as a remedy for fever, malaria, and inflammation. According to TCM theory, *A. annua* is characterized by a cold property and is believed to exert a "cooling the blood and hemostatic" effect. It has been employed in managing bleeding symptoms associated with thrombocytopenia and coagulation disorders, such as purpura and epistaxis. Fresh *A. annua* is often consumed as a decoction or topically applied in mashed form to bleeding sites to alleviate hemorrhagic symptoms [18, 19]. Despite its long-standing empirical use in bleeding-related conditions, *A. annua* has not been previously investigated in the context of hematopoietic regulation from a modern pharmacological perspective.

In the present study, chemical profiling of *A. annua* identified multiple bioactive constituents, consistent with prior phytochemical reports. Notably, *A. annua* extract was found to enhance MK differentiation and maturation in both hematopoietic cell lines, demonstrated by increased CD41/CD42b expression and DNA polyploidization—key features of terminal megakaryocytic differentiation.

We further employed network pharmacology to explore its multi-target regulatory profile. The analysis identified 21 phytoconstituents within *A. annua* that collectively targeted 46 core genes associated with thrombocytopenia. These targets were significant involved in several critical pathways, including IL-17, estrogen, MAPK, and JAK/STAT cascades—all of which are intimately linked to MK development and platelet production [7, 27, 36]. Notably, PI3K/Akt, JAK/STAT, and MAPK signaling pathways represent the principal downstream effectors of TPO/c-MPL signaling, which orchestrates MK proliferation, endomitosis, maturation, and platelet release [7]. Dysregulation of these pathways has been implicated in various forms of acquired or congenital thrombocytopenia, underscoring their therapeutic relevance [7, 8]. The potential for botanical compounds to modulate these canonical pathways is supported by accumulating pharmacological evidence. For instance, our previous studies identified 3,4,3′-tri-O-methylellagic acid (TMEA), a phytochemical derived from *Sanguisorba officinalis* L., as a novel small-molecule c-MPL agonist



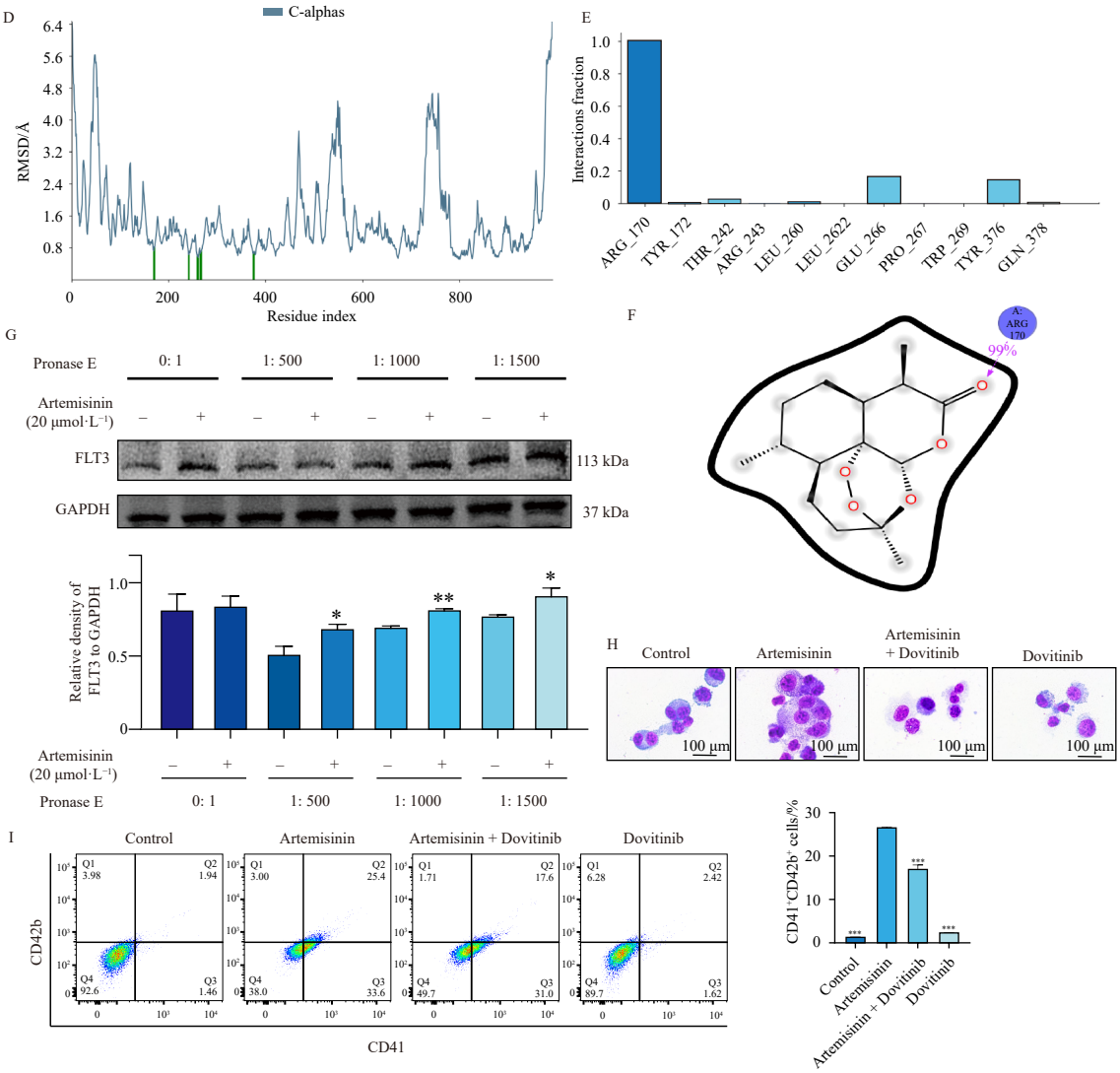


Fig. 9 Artemisinin directly interacts with FLT3 to promote MK differentiation. (A) Molecular docking analysis showing the predicted binding conformation of artemisinin within the FLT3 active site. (B) RMSD profiles of the FLT3 backbone (blue) and the ligand artemisinin (red) during 100 ns molecular dynamics simulation. (C) RMSF values of individual ligand atoms fitted on the protein backbone throughout the simulation. (D) RMSF values of FLT3 residues illustrating conformational stability of the binding site region. (E) Hydrogen bond occupancy analysis demonstrating a persistent interaction between artemisinin and ARG170. (F) Two-dimensional schematic representation of the protein–ligand interaction network, highlighting hydrogen bonds and hydrophobic contacts. (G) DARTS assay showing that artemisinin treatment protects FLT3 from pronase E-mediated degradation in K562 cells (n = 3). (H) Giemsa staining of K562 cells treated with artemisinin (10 μmol·L^{-1}), dovitinib (0.8 μmol·L^{-1}), or their combination for 5 days. Scale bar = 100 μm. (I) Flow cytometry analysis of CD41^{+}CD42b^{+} cells following treatment as indicated (n = 3). Data are presented as mean ± SD. For G, statistical significance was determined using unpaired Student's t-test, $^{*}P < 0.05$, $^{**}P < 0.01$ *vs* the corresponding Pronase E-treated group (without artemisinin); for I, one-way ANOVA was used. $^{***}P < 0.001$ *vs* artemisinin group.

that activates PI3K/Akt and MAPK signaling, thereby promoting MK differentiation and platelet recovery in RIT models [37]. Similarly, genistin, a naturally occurring isoflavone with estrogen-like activity, was shown to activate ERβ and its downstream Akt and ERK pathways, facilitating platelet production and exerting therapeutic effects in RIT models [26]. These findings collectively reinforce the concept that structurally diverse natural compounds can converge on shared intracellular pathways to modulate thrombopoiesis. In this context, the multi-component nature of *A. annua* may offer a unique pharmacological advantage. Unlike single-compound agents, *A. annua* comprises a complex mixture of bioactive molecules, each potentially engaging distinct but complementary targets. This multi-target paradigm may result in a synergistic enhancement of MK lineage commitment and platelet formation via concurrent modulation of multiple signaling axes. Such a mechanism could not only amplify therapeutic efficacy but also reduce the likelihood of resistance associated with monotherapies. Given the enrichment of *A. annua* targets within several thrombopoiesis-related pathways, it is plausible that the integrated action of its phytochemical constituents underlies its robust thrombopoietic activity observed in cellular models. Future studies dissecting the individual and combinatorial effects of key constituents within *A. annua* on specific targets and signaling nodes will be essential to fully delineate its mechanistic landscape and therapeutic potential. Nevertheless, it should be acknowledged that the present study did not fully resolve the contribution of each constituent in *A. annua* or their potential synergistic or antagonistic interactions. Although artemisinin showed the strongest MK differentiation-promoting activity among the representative constituents screened in vitro, this does not exclude the possibility that other compounds may contribute to the overall thrombopoietic effect of *A. annua in vivo*. Some constituents with modest or limited activity in isolated cell-based assays may still participate through indirect mechanisms, such as protecting the BM microenvironment, reducing radiation-induced oxidative stress or apoptosis, regulating inflammatory responses, improving pharmacokinetic behavior, or modulating parallel hematopoietic pathways. In addition, additive, synergistic, or antagonistic interactions among different constituents may influence the final pharmacological effect of the whole herb. There-

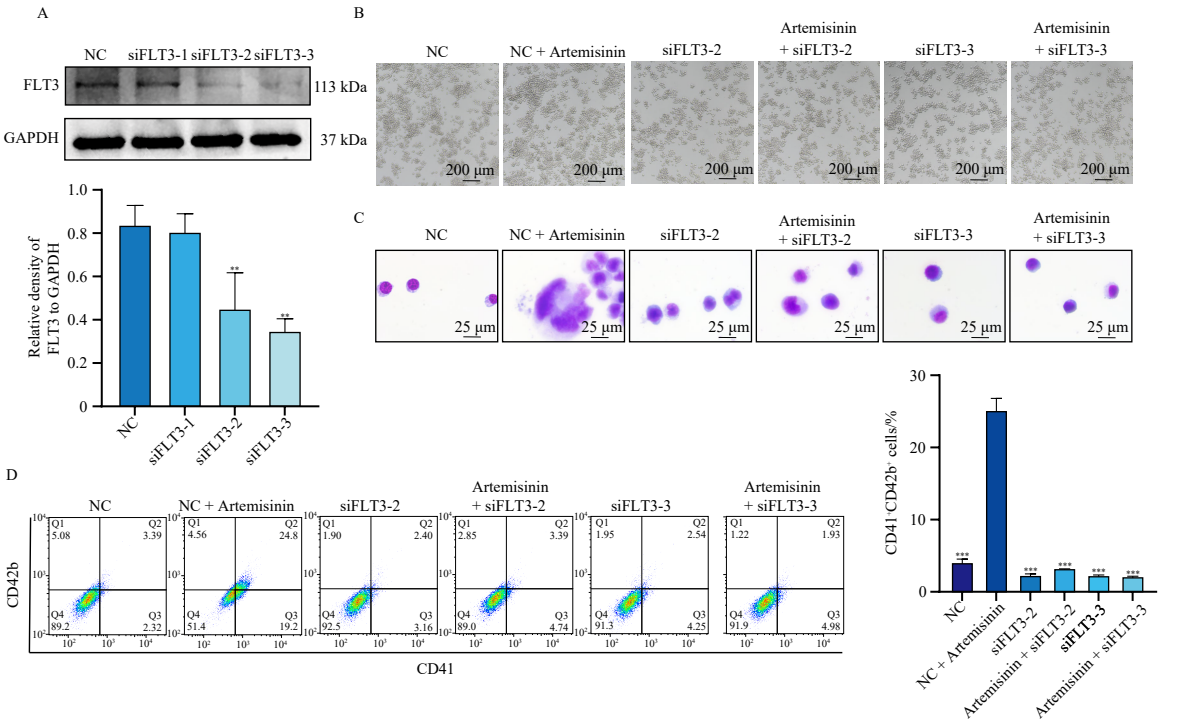
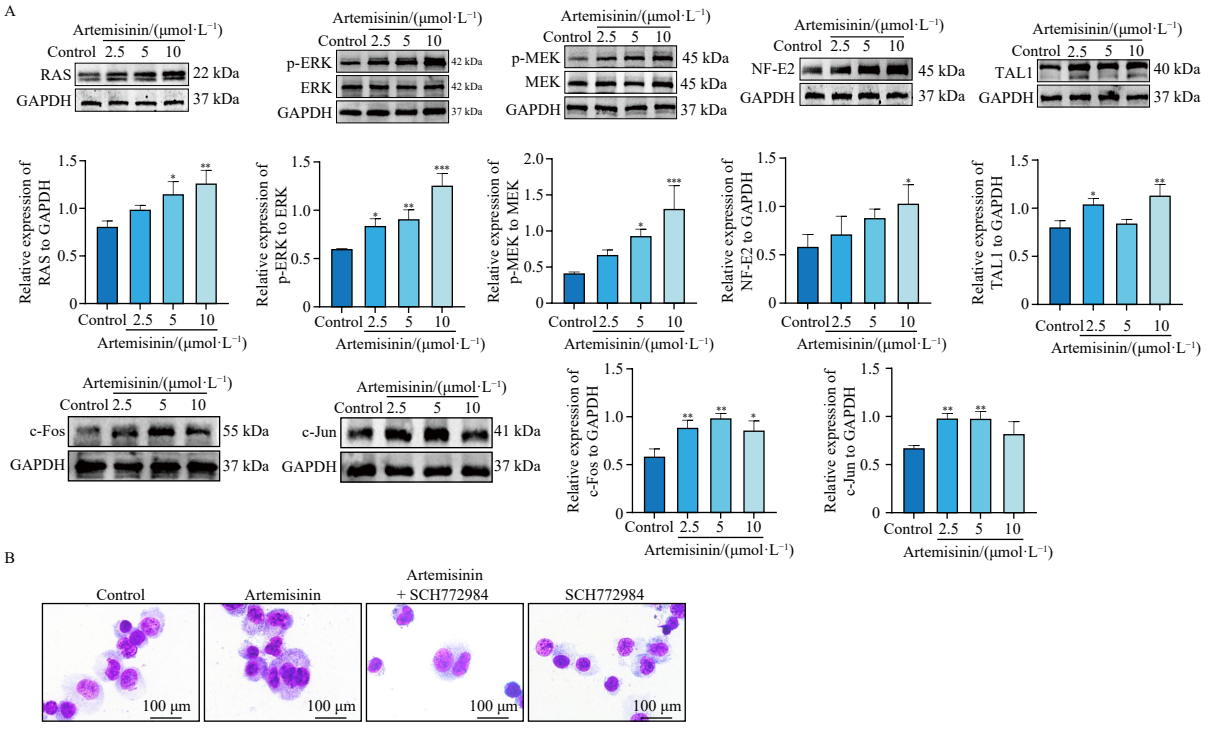


Fig. 10 FLT3 knockdown attenuates artemisinin-induced MK differentiation in K562 cells. (A) Western blot analysis of FLT3 protein expression in K562 cells transfected with negative control siRNA (NC) or three independent FLT3 siRNAs (siFLT3-1, siFLT3-2, and siFLT3-3). GAPDH was used as the loading control. Quantitative analysis showed the relative density of FLT3 normalized to GAPDH (n = 3). $^{**}P < 0.01$ *vs* NC group. (B) Light microscopy images showing morphological changes in K562 cells after FLT3 knockdown with or without artemisinin treatment. Scale bar = 200 μm. (C) Giemsa staining of K562 cells showing cell morphology and nuclear changes after FLT3 knockdown with or without artemisinin treatment. Scale bar = 25 μm. (D) Representative flow cytometric plots showing CD41 and CD42b expression in K562 cells after FLT3 knockdown with or without artemisinin treatment. Quantitative analysis of $CD41^+CD42b^+$ cells in K562 cells after FLT3 knockdown with or without artemisinin treatment (n = 3). $^{***}P < 0.001$ *vs* NC + Artemisinin group. Data are presented as mean ± SD from three independent experiments. Statistical significance was determined by one-way ANOVA.

fore, artemisinin should be regarded as a principal active constituent identified in the present study, rather than the only pharmacologically relevant component of *A. annua*. Further studies using different fractions of *A. annua*, combinations of major constituents, and *in vivo* validation models will be necessary to clarify the integrated multi-component and multi-target mechanisms underlying the thrombopoietic activity of *A. annua*.

Having established the chemical composition of *A. annua* and confirmed its thrombopoietic efficacy in vitro, we next sought to identify the principal bioactive constituents responsible for its hematopoietic activity. Bioactivity-guided screening revealed that artemisinin, one of the major phytochemicals in *A. annua*, exhibited robust effects on megakaryocytic differentiation and maturation across multiple in vitro models. Specifically, artemisinin sig-



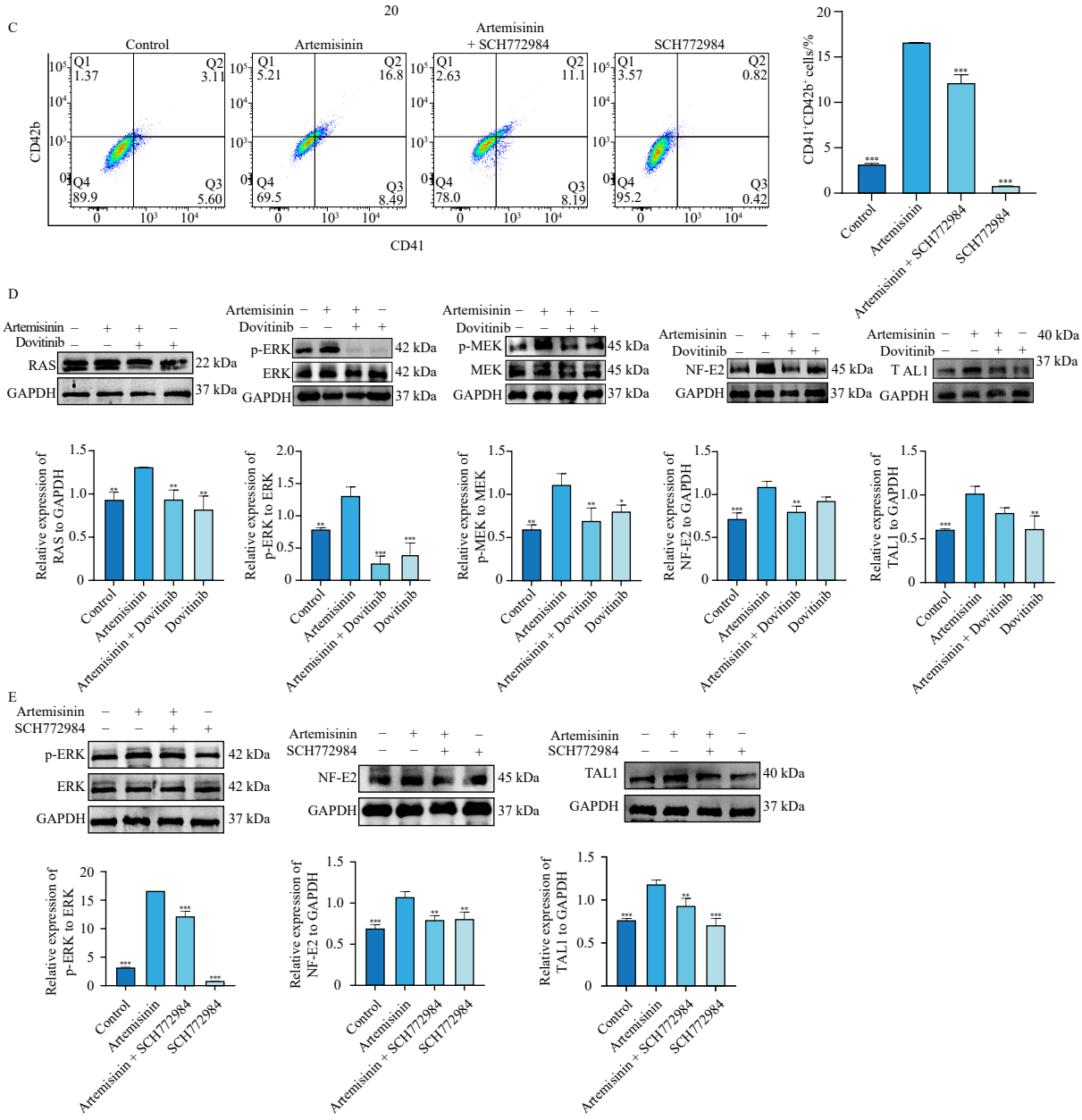


Fig. 11 Artemisinin promotes MK differentiation *via* FLT3-dependent activation of the MAPK signaling pathway. (A) Western blot analysis of RAS, p-MEK, p-ERK, NF-E2, TAL1, c-Fos, and c-Jun protein levels in K562 cells following artemisinin treatment (2.5, 5, and 10 μmol·L^{-1}) (n = 3). (B) Giemsa staining of K562 cells treated with artemisinin, SCH772984 (1 μmol·L^{-1}), or their combination for 5 days. Scale bar = 100 μm. (C) Flow cytometry analysis of CD41^{+}CD42b^{+} cells following treatment as indicated (n = 3). (D) Western blot analysis showing that dovitinib (0.8 μmol·L^{-1}) inhibits artemisinin-induced phosphorylation of MEK and ERK and reduces expression of NF-E2 and TAL1 in K562 cells (n = 3). (E) Western blot analysis demonstrating that SCH772984 suppresses ERK activation and attenuates the artemisinin-mediated upregulation of NF-E2 and TAL1 (n = 3). Data are presented as mean ± SD. For A and B, statistical significance was determined using one-way ANOVA, $^{*}P < 0.05$, $^{**}P < 0.01$, $^{***}P < 0.001$ *vs* Control group; for C-E, one-way ANOVA was used, $^{*}P < 0.05$, $^{**}P < 0.01$, $^{***}P < 0.001$ *vs* artemisinin group.

nificantly promoted MK differentiation in Meg-01 and K562 cell lines, and in murine HSPCs. This was evidenced by increased cell size, enhanced nuclear lobulation, upregulation of lineage-specific markers (CD41, CD42b, CD61), elevated DNA ploidy, and an increased yield of platelet-like particles. Importantly, artemisinin did not induce cytotoxicity under the experimental conditions, as demonstrated by unchanged LDH release. These findings confirm that artemisinin drives MK lineage commitment and terminal maturation while preserving cell viability.

Encouraged by the *in vitro* data, we further evaluated the potential efficacy of artemisinin *in vivo*. Consistent with its *in vitro* activity, artemisinin significantly accelerated platelet recovery during the nadir and rebound phases post-irradiation. Notably, in contrast to TPO, artemisinin restored platelet levels to a physiological range without inducing thrombocytosis at later time points, such as day 17. This distinction is clinically relevant, as TPO analogs can lead to thrombotic events due to excessive platelet production [32]. The ability of artemisinin to normalize platelet counts without overshooting baseline values suggests a more physiologically balanced regulatory effect on megakaryopoiesis and platelet homeostasis. Comprehensive *in vivo* safety assessments further support the translational potential of artemisinin. Treatment did not induce significant changes in body weight, organ coefficients, or histological architecture of major organs. Moreover, serum biochemical indices of hepatic, renal, and cardiac function remained within normal ranges, confirming the absence of systemic toxicity at the therapeutic dose. Mechanistically, the hematopoietic restoration observed following artemisinin treatment appears to be mediated, at least in part, through attenuation of radiation-induced BM injury. Apoptotic analyses revealed that artemisinin significantly suppressed irradiation-induced apoptosis in BM cells, as shown by reduced An-

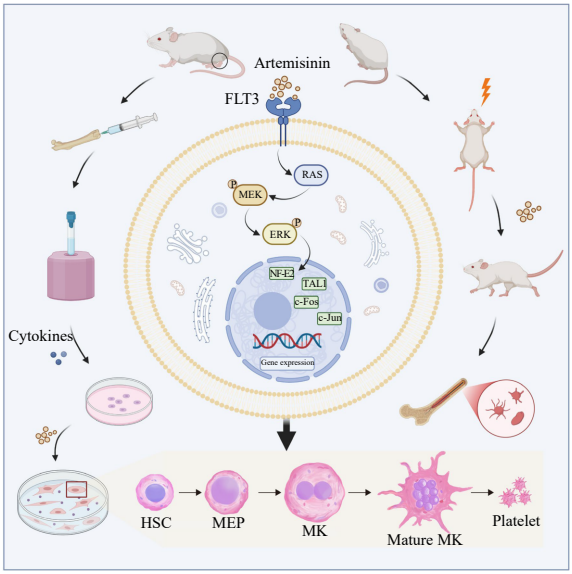


Fig. 12 Schematic illustration of the molecular mechanism of artemisinin action.

nexin V positivity and downregulation of pro-apoptotic markers Bax and Caspase-3 [38]. In parallel, γ-H2AX expression—a well-recognized indicator of DNA double-strand lesions [39]—was markedly reduced in artemisinin-treated mice, indicating mitigation of radiation-induced genomic damage. These findings collectively suggest that artemisinin preserves BM integrity by inhibiting apoptosis and promoting DNA damage repair, thereby contributing to the overall recovery of hematopoiesis. Given that platelets are terminally derived from MKs, we next examined the upstream events contributing to thrombopoietic recovery. Histological analysis revealed a substantial increase in BM MK numbers following artemisinin treatment, supporting the hypothesis that enhanced thrombopoiesis resulted from stimulated megakaryopoiesis. Further flow cytometric profiling indicated that artemisinin not only restored the population of HSPCs ($CD34^+c\text{-}Kit^+$) but also significantly increased the frequency of megakaryocytic progenitors ($c\text{-}Kit^+CD41^+$), suggesting that artemisinin promotes both progenitor expansion and lineage-specific differentiation. In accordance, artemisinin elevated MK maturation markers' expression, increased MK polyploidy, and augmented production of circulating reticulated platelets. These effects reflect coordinated stimulation of MK proliferation, differentiation, and proplatelet formation, highlighting the multi-stage activity of artemisinin across the entire megakaryopoietic continuum. Beyond quantitative enhancement of platelet numbers, artemisinin also restored platelet functionality in irradiated mice. This was demonstrated by shortened tail bleeding time, improved clot retraction in whole blood, and increased levels of reticulated platelets. These findings confirm that artemisinin not only promotes the production of platelets but also preserves or restores their hemostatic competence, which is critical for effective clinical translation. In summary, artemisinin exerts multifaceted therapeutic effects in RIT by promoting HSPC expansion, enhancing MK differentiation and maturation, accelerating platelet recovery, reducing BM apoptosis and DNA damage, and restoring platelet function.

Network pharmacology and molecular docking simulations were employed to predict direct target of artemisinin. Among the top-ranked candidates, FLT3 emerged as a high-affinity binding partner of artemisinin. This computational prediction was experimentally substantiated using DARTS assays, which demonstrated a significant stabilization of FLT3 in the presence of artemisinin, indicating a direct physical interaction in the cellular context. To determine the functional relevance of FLT3 activation, we employed the selective FLT3 inhibitor dovitinib in differentiation assays. Co-treatment with dovitinib significantly attenuated the morphological and molecular features of artemisinin-induced MK differentiation, including reduced expression of CD41 and CD42b, thus confirming that FLT3 activation is functionally required for the differentiation-promoting effects of artemisinin. To further strengthen this conclusion, siRNA-mediated FLT3 knockdown was performed in K562 cells. FLT3 knockdown attenuated artemisinin-induced megakaryocytic morphological changes and markedly reduced the increase in $CD41^+CD42b^+$ cells. These genetic loss-of-function results further support the functional involvement of FLT3 in artemisinin-induced MK differentiation and complement the pharmacological evidence obtained with dovitinib. FLT3 is essential for hematopoiesis. Its activation by the FLT3 ligand triggers autophosphorylation and activates MAPK pathway—which regulate hematopoietic cell survival, proliferation, and lineage commitment [25, 28, 29]. Within the megakaryopoietic lineage, FLT3 has been shown to synergize with TPO to promote MK progenitors development [40, 41]. Our findings thus place artemisinin as a novel small-molecule modulator of FLT3, capable of promoting thrombopoiesis via FLT3 activation. Interestingly, while dovitinib markedly reduced the effects of artemisinin, it did not completely abolish MK differentiation, suggesting that artemisinin may exert its effects through additional targets. This partial blockade highlights the need for comprehensive target identification using advanced techniques such as chemical proteomics (e.g., affinity-based pull-down assays coupled with mass spectrometry) [42], which could further elucidate the full spectrum of artemisinin's molecular interactions. In parallel, our network pharmacology analysis predicted that the MAPK signaling pathway may represent a critical downstream effector of artemisinin. Consistently, artemisinin treatment upregulated RAS expression and enhanced MEK and ERK phosphorylation in K562 cells. These effects were accompanied by elevated expression of NF-E2 and TAL1, both of which are important to MK development. Importantly, inhibition of ERK using SCH772984 abrogated artemisinin-induced expression of differentiation markers and transcription factors, confirming the pivotal role of MAPK signaling in this process. To establish the hierarchical relationship between FLT3 and MAPK activation, we assessed the impact of FLT3 inhibition on MAPK signaling. Dovitinib treatment suppressed artemisinin-induced upregulation of RAS, MEK and ERK phosphorylation, and NF-E2 and TAL1, indicating that MAPK signaling operates downstream of FLT3. Although our previous study also identified FLT3 as a thrombopoietic regulatory target of bavachinin A [25], the present work provides a distinct and complementary mechanism. Bavachinin A is a prenylated flavonoid derived from Fructus Psoraleae and was shown to promote MK differentiation mainly through the FLT3–PI3K/Akt pathway [25]. In contrast, artemisinin is a sesquiterpene lactone derived from *A. annua* with a unique endoperoxide bridge. Our docking and molecular dynamics analyses suggest that artemisinin interacts with FLT3 through a different binding mode, with ARG170 serving as a key residue mediating the artemisinin–FLT3 interaction, whereas bavachinin A was previously predicted to interact with FLT3 mainly through CYS694. Functionally, artemisinin activates the FLT3/MAPK axis, leading to MEK/ERK phosphorylation and upregulation of NF-E2 and TAL1. Thus, although FLT3 is a shared upstream node, the two studies differ in herbal source, active compound, chemical scaffold, binding residue, and downstream signaling output. These findings suggest that structurally distinct natural compounds may modulate FLT3 through different binding modes and pathway-biased signaling mechanisms, thereby expanding the pharmacological understanding of FLT3 as a druggable regulatory hub in thrombopoiesis.

Taken together, these findings delineate a mechanistic pathway wherein artemisinin directly binds and activates FLT3, sub-

sequently triggering the MAPK cascade and activating hematopoietic transcription factors, ultimately driving MK differentiation and platelet production.

5. Conclusion

In the present study, we identified its principal bioactive constituent, artemisinin, as a potent inducer of MK differentiation and thrombopoiesis. Through *in vitro* cellular models and *in vivo* RIT murine models, artemisinin was shown to enhance MK maturation, promote platelet biogenesis, and ameliorate hematopoietic injury without inducing systemic toxicity. Mechanistically, artemisinin exerts its effects *via* direct interaction with FLT3, activating MAPK signaling cascade and lineage-specific transcription factors critical for MK development. These findings not only elucidate a novel molecular mechanism underlying the hematopoietic activity of artemisinin but also identify FLT3 as a previously unrecognized target in megakaryopoietic regulation. Given its well-established clinical safety profile and oral bioavailability, artemisinin represents a promising therapeutic candidate for thrombocytopenia, particularly in radiation-related hematopoietic injuries. Moreover, we underscores broader efficacy of traditional herbal compounds as a rich source for the discovery of novel hematopoietic modulators and offers a basis to advance artemisinin into clinical practice in supportive care for hematological disorders.

Funding

This work was supported by the Joint Project of Luzhou Municipal People's Government and Southwest Medical University (Nos. 2025LZXNYDZH06, 2024LZXNYDJ030), the Sichuan Provincial Natural Science Foundation General Project (Nos. 2024NSFSC0711, 2023NSFSC0657), the National Science Foundation of China (Nos. 82204666, 82074129, 81774013 and 82273889), the Science and Technology Program Joint Innovation Project of Sichuan Province (Nos. 2022YFS0635 and 2022YFS0635-B1), and the National Innovation and Entrepreneurship Training Program for College Students of China (Nos. 202410632006, 202310632102 and S202310632303).

Data availability

The original contributions presented in the study are included in the article Material, further inquiries can be directed to the corresponding author.

Declarations of any conflicts of interest

The authors declare that the research was conducted in the absence of any commercial or financial relationships that could be construed as a potential conflict of interest.

References

1 Guo H, Chou WC, Lai Y, et al. Multi-omics analyses of radiation survivors identify radioprotective microbes and metabolites. *Science*. 2020;370(6516):eaay9097. https://doi.org/10.1126/science.aay9097.
2 Zhang L, Xu W, Zeng Y, et al. Astragaloside IV accelerates hematopoietic reconstruction by improving the AMPK/PGC1α-mediated mitochondrial function in hematopoietic stem cells. *Chin Med*. 2025;20(1):44. https://doi.org/10.1186/s13020-025-01092-3.
3 Huang M, Ye A, Zhang H, et al. Siwu Decoction mitigates radiation-induced immune senescence by attenuating hematopoietic damage. *Chin Med*. 2024;19(1):167. https://doi.org/10.1186/s13020-024-01036-3.
4 Xu Y, Wang S, Shen MQ, et al. hGH promotes megakaryocyte differentiation and exerts a complementary effect with c-Mpl ligands on thrombopoiesis. *Blood*. 2014;123(14):2250-2260. https://doi.org/10.1182/blood-2013-09-525402.
5 Singh VK, Seed TM. Pharmacological management of ionizing radiation injuries: current and prospective agents and targeted organ systems. *Expert Opin Pharmacother*. 2020;21(3):317-337. https://doi.org/10.1080/14656566.2019.1702968.
6 Furniss JA, Tarassova N, Poole AWJB. Platelet generation *in vivo* and *in vitro*. *Blood*. 2024;144(22):2283-2294. https://doi.org/10.1182/blood.2024024601.
7 Eto K, Kunishima S. Linkage between the mechanisms of thrombocytopenia and thrombopoiesis. *Blood*. 2016;127(10):1234-1241. https://doi.org/10.1182/blood-2015-07-607903.
8 Bianchi E, Norfo R, Pennucci V, et al. Genomic landscape of megakaryopoiesis and platelet function defects. *Blood*. 2016;127(10):1249-1259. https://doi.org/10.1182/blood-2015-07-607952.
9 Noetzli LJ, French SL, Machlus KR. New insights into the differentiation of megakaryocytes from hematopoietic progenitors. *Arterioscler Thromb Vasc Biol*. 2019;39(7):1288-1300. https://doi.org/10.1161/ATVBAHA.119.312129.
10 Machlus KR, Johnson KE, Kulenthirarajan R, et al. CCL5 derived from platelets increases megakaryocyte proplatelet formation. *Blood*. 2016;127(7):921-926. https://doi.org/10.1182/blood-2015-05-644583.
11 Yang F, Lai J, Deng J, et al. The application of ethnomedicine in modulating megakaryocyte differentiation and platelet counts. *Int J Mol Sci*. 2023;24(4):3168. https://doi.org/10.3390/ijms24043168.
12 Chen W, Zhu LJ, Wang L, et al. A novel antithrombocytopenia agent, Rhizoma Cibotii, promotes megakaryopoiesis and thrombopoiesis through the PI3K/AKT, MEK/ERK, and JAK2/STAT3 signaling pathways. *Int J Mol Sci*. 2022;23(22):14060. https://doi.org/10.3390/ijms232214060.
13 Yang X, Wang L, Zeng J, et al. Caulis polygoni multiflori accelerates megakaryopoiesis and thrombopoiesis *via* activating PI3K/akt and MEK/ERK signaling pathways. *Pharmaceuticals (Basel)*. 2022;15(10):1204. https://doi.org/10.3390/ph15101204.
14 Ming HL, Wen HL, Ming QH. Professor Qiu Heming's case study on treating blood diseases with *Artemisia annua* and Biejia Decoction. *J New Chin Med*. 2004;36(7):27-28. https://doi.org/10.3969/j.issn.0256-7415.2004.07.003.
15 Luo W. Clinical experience of modified *Artemisia annua* and Biejia Decoction in the treatment of hematological diseases. *J Pract Tradit Chin Med*. 2007;23(9):7-8. https://doi.org/10.3969/j.issn.1004-2814.2007.09.048.
16 Gong J. The anti-leukemia effect of artemisinin and its derivatives. *Int J Blood Transfus Hematol*. 2007;30(3):264-266. https://doi.org/10.3760/cma.j.issn.1673-419X.2007.03.017.
17 Wang BC, Sui J, Yu ZW, et al. Screening the hemostatic active fraction of *Artemisia annua* L. *in-vitro*. *Iran J Pharm Res*. 2011;10(1):57.
18 Huang ZY, Fan B, Mao WW, et al. Topical application of *Artemisia annua* L. essential oil ameliorates 2, 4-dintrochlorobenzene-induced atopic dermatitis in mice. *J Ethnopharmacol*. 2024;333:118439. https://doi.org/10.1016/j.jep.2024.118439.
19 Zhao XW, Dai X, Wang FY, et al. *Artemisia annua* L. leaf extracts suppress influenza virus infection by targeting the viral nucleoprotein and blocking mitochondria-mediated apoptosis. *Virol Sin*. 2025;40(2):247-59. https://doi.org/10.1016/j.virs.2025.03.001.
20 Liang D, Xuan DY, Liu Chang, et al. Mechanism of *Artemisia annua* L. in the treatment of acute myocardial infarction: network pharmacology, molecular docking and *in vivo* validation. *Mol Divers*. 2024;28:3225-3342. https://doi.org/10.1007/s11030-023-10750-3.
21 Gao P, Wang JY, Qiu C, et al. Photoaffinity probe-based antimalarial target identification of artemisinin in the intraerythrocytic developmental cycle of Plasmodium falciparum. *iMeta*. 2024;3(2):e176. https://doi.org/10.1002/imt2.176.
22 Lim HS, Park G. Artemisinin protects dopaminergic neurons against 1-methyl-4-phenyl-1, 2, 3, 6-tetrahydropyridine-induced neurotoxicity in a mouse model of Parkinson's disease. *Biomed Pharmacother*. 2024;170:115972. https://doi.org/10.1016/j.biopha.2023.115972.
23 Liu Y, Jiang JJ, Du SY, et al. Artemisinins ameliorate polycystic ovarian syndrome by mediating LONP1-CYP11A1 interaction. *Science*. 2024;384(6701):eadk5382. https://doi.org/10.1126/science.adk5382.
24 Wang L, Liu S, Luo JS, et al. Targeting a thrombopoietin-independent strategy in the discovery of a novel inducer of megakaryocytopoiesis, DMAG, for the treatment of thrombocytopenia. *Haematologica*. 2022;108(5):1394. https://doi.org/10.3324/haematol.2022.282209.
25 Wang L, Zhang T, Yang X, et al. Multimodal discovery of bavachinin A: a natural FLT3 agonist for treating thrombocytopenia. *Phytomedicine*. 2025;140:156597. https://doi.org/10.1016/j.phymed.2025.156597.
26 Tang XQ, Liao R, Zhou L, et al. Genistin: a novel estrogen analogue targeting ERβ to alleviate thrombocytopenia. *Int J Biol Sci*. 2024;20(6):2236. https://doi.org/10.7150/ijbs.90483.
27 Huang M, Wang L, Zhang QH, et al. Interleukins in platelet biology: unraveling the complex regulatory network. *Pharmaceuticals (Basel)*. 2024;17(1):109. https://doi.org/10.3390/ph17010109.
28 Chu SH, Heiser D, Li L, et al. FLT3-ITD knockin impairs hematopoietic stem cell quiescence/homeostasis, leading to myeloproliferative neoplasm. *Cell Stem Cell*. 2012;11(3):346-358. https://doi.org/10.1016/j.stem.2012.05.027.

29 Stirewalt DL, Radich JP. The role of FLT3 in haematopoietic malignancies. *Nat Rev Cancer*. 2003;3:650-665. https://doi.org/10.1038/nrc1169.

30 Tkaczynski E, Arulselvan A, Tkaczynski J, et al. 2-O, 3-O desulfated heparin mitigates murine chemotherapy-and radiation-induced thrombocytopenia. *Blood Adv*. 2018;2(7):754-761. https://doi.org/10.1182/bloodadvances.2017013672.

31 Barazzuol L, Coppes RP, Luijk Pv. Prevention and treatment of radiotherapy-induced side effects. *Mol Oncol*. 2020;14(7):1538-1554. https://doi.org/10.1002/1878-0261.12750.

32 Ghanima W, Cooper N, Rodeghiero F, et al. Thrombopoietin receptor agonists: ten years later. *Haematologica*. 2019;104(6):1112. https://doi.org/10.3324/haematol.2018.212845.

33 Poston JN, Gernsheimer TB. Glucocorticoids promote response to thrombopoietin-receptor agonists in refractory ITP: a case series. *Int J Hematol*. 2019;110(2):255-259. https://doi.org/10.1007/s12185-019-02638-6.

34 Catalá-López F, Corrales I, de la Fuente-Honrubia C, et al. Risk of thromboembolism with thrombopoietin receptor agonists in adult patients with thrombocytopenia: systematic review and meta-analysis of randomized controlled trials. *Med Clin (Barc)*. 2015;145(12):511-519. https://doi.org/10.1016/j.medcli.2015.03.014.

35 Liu YQ, Wang XL, He DH, et al. Protection against chemotherapy-and radiotherapy-induced side effects: a review based on the mechanisms and therapeutic opportunities of phytochemicals. *Phytomedicine*. 2021;80:153402. https://doi.org/10.1016/j.phymed.2020.153402.

36 Du C, Xu Y, Yang K, et al. Estrogen promotes megakaryocyte polyploidization *via* estrogen receptor beta-mediated transcription of GATA1. *Leukemia*. 2017;31(4):945-956. https://doi.org/10.1038/leu.2016.285.

37 Jiang XQ, Sun YS, Yang S, et al. Novel chemical-structure TPOR agonist, TMEA, promotes megakaryocytes differentiation and thrombopoiesis *via* mTOR and ERK signalings. *Phytomedicine*. 2023;110:154637. https://doi.org/10.1016/j.phymed.2022.154637.

38 Yang S, Wang L, Wu YS, et al. Apoptosis in megakaryocytes: safeguard and threat for thrombopoiesis. *Front Immunol*. 2023;13:1025945. https://doi.org/10.3389/fimmu.2022.1025945.

39 Sekikawa Y, Kato TA. Radiation-induced Gamma-H2AX foci staining and analysis. In: TA Kato, eds. DNA damage detection: methods and protocols. New York, NY:Humana Press; 2025:25-29. https://doi.org/10.1007/978-1-0716-4574-1_4.

40 Behrens K, Alexander WS. Cytokine control of megakaryopoiesis. *Growth Factors*. 2018;36(3-4):89-103. https://doi.org/10.1080/08977194.2018.1498487.

41 Sun SJ, Wang WJ, Latchman Y, et al. Expression of plasma membrane receptor genes during megakaryocyte development. *Physiol Genomics*. 2013;45(6):217-227. https://doi.org/10.1152/physiolgenomics.00056.2012.

42 Chen X, Wang YT, Ma N, et al. Target identification of natural medicine with chemical proteomics approach: probe synthesis, target fishing and protein identification. *Signal Transduct Target Ther*. 2020;5(1):72. https://doi.org/10.1038/s41392-020-0186-y.